12-2010

A Potential Vorticity Theory for the Formation of Elongate Channels in River Deltas and Lakes

Federico Falcini

Douglas J. Jerolmack
University of Pennsylvania, sediment@sas.upenn.edu

Recommended Citation
Falcini, F., & Jerolmack, D. J. (2010). A Potential Vorticity Theory for the Formation of Elongate Channels in River Deltas and Lakes. *Journal of Geophysical Research: Earth Surface, 115* (F4), F04038-. http://dx.doi.org/10.1029/2010JF001802

A Potential Vorticity Theory for the Formation of Elongate Channels in River Deltas and Lakes

Abstract
Rivers empty into oceans and lakes as turbulent sediment-laden jets, which can be characterized by a Gaussian horizontal velocity profile that spreads and decays downstream because of shearing and lateral mixing at the jet margins. Recent experiments demonstrate that this velocity field controls river-mouth sedimentation patterns. In nature, diffuse jets are associated with mouth bar deposition forming bifurcating distributary networks, while focused jets are associated with levee deposition and the growth of elongate channels that do not bifurcate. River outflows from elongate channels are similar in structure to cold filaments observed in ocean currents, where high potential vorticity helps to preserve coherent structure over large distances. Motivated by these observations, we propose a hydrodynamic theory that seeks to predict the conditions under which elongate channels form. Our approach models jet velocity patterns using the flow vorticity. Both shearing and lateral spreading are directly related to the vertical component of vorticity. We introduce a new kind of potential vorticity that incorporates sediment concentration and thus allows study of jet sedimentation patterns. The potential vorticity equation reduces the number of fluid momentum equations to one without losing generality. This results in a compact analytical solution capable of describing the streamwise evolution of the potential vorticity of a sediment-laden jet from initial conditions at the river mouth. Our theory predicts that high potential vorticity is a necessary condition for focused levee deposition and the creation of elongate channels. Comparison to numerical, laboratory, and field studies indicates that potential vorticity is a primary control on channel morphology. Our results may be useful for designing river delta restoration schemes such as the proposed Mississippi Delta diversion.

Keywords
river channel dynamics, river jets, sediment transport

Disciplines
Earth Sciences | Environmental Sciences | Geomorphology | Physical Sciences and Mathematics | Sedimentology

A potential vorticity theory for the formation of elongate channels in river deltas and lakes

Federico Falcini[1] and Douglas J. Jerolmack[1]

Received 19 June 2010; revised 5 October 2010; accepted 14 October 2010; published 21 December 2010.

[1] Rivers empty into oceans and lakes as turbulent sediment-laden jets, which can be characterized by a Gaussian horizontal velocity profile that spreads and decays downstream because of shearing and lateral mixing at the jet margins. Recent experiments demonstrate that this velocity field controls river-mouth sedimentation patterns. In nature, diffuse jets are associated with mouth bar deposition forming bifurcating distributary networks, while focused jets are associated with levee deposition and the growth of elongate channels that do not bifurcate. River outflows from elongate channels are similar in structure to cold filaments observed in ocean currents, where high potential vorticity helps to preserve coherent structure over large distances. Motivated by these observations, we propose a hydrodynamic theory that seeks to predict the conditions under which elongate channels form. Our approach models jet velocity patterns using the flow vorticity. Both shearing and lateral spreading are directly related to the vertical component of vorticity. We introduce a new kind of potential vorticity that incorporates sediment concentration and thus allows study of jet sedimentation patterns. The potential vorticity equation reduces the number of fluid momentum equations to one without losing generality. This results in a compact analytical solution capable of describing the streamwise evolution of the potential vorticity of a sediment-laden jet from initial conditions at the river mouth. Our theory predicts that high potential vorticity is a necessary condition for focused levee deposition and the creation of elongate channels. Comparison to numerical, laboratory, and field studies indicates that potential vorticity is a primary control on channel morphology. Our results may be useful for designing river delta restoration schemes such as the proposed Mississippi Delta diversion.

Citation: Falcini, F., and D. J. Jerolmack (2010), A potential vorticity theory for the formation of elongate channels in river deltas and lakes, *J. Geophys. Res.*, *115*, F04038, doi:10.1029/2010JF001802.

1. Introduction

[2] Sediment-charged rivers discharging into oceans and lakes often generate spectacular sediment plumes (Figure 1). If the turbulent jet is not strongly disrupted by waves or tides, focused sedimentation at its margins may confine flow such that the river mouth progrades basinward [*Wright*, 1977; *Edmonds and Slingerland*, 2007]. A good example is the Mississippi River Delta, which shows that such prograding channels may take a variety of forms even under similar environmental conditions (Figure 2). A man-made diversion from the Atchafalaya branch of the Mississippi has resulted in the rapid growth of the Wax Lake Delta (Figure 2), which now serves as an important prototype for planned restoration schemes in the vicinity of New Orleans [*Parker and Sequeiros*, 2006; *Kim et al.*, 2009a; *Edmonds and Slingerland*, 2007, 2010]. Wax Lake channel growth appears to occur by two simultaneous processes [*Edmonds and Slingerland*, 2007]: (1) deposition at jet margins leads to levee progradation and channel elongation while (2) deposition and vertical aggradation of a mouth bar in the jet centerline enhances flow divergence leading to bifurcation. The repetitive branching network that results from these processes is the most common channel pattern seen on the shorelines of fluvially dominated deltas [*Edmonds and Slingerland*, 2007; *Jerolmack and Swenson*, 2007].

[3] A much less common morphology is the famous Balize lobe to the east on the Mississippi Delta, generally referred to as the "birdsfoot" (Figure 2). Its morphology indicates that channels somehow prograde great distances without bifurcating [*Kim et al.*, 2009b]. This is particularly evident in the Southwest Pass channel (Figure 2) where, despite dimensions and water discharges comparable to the Wax Lake feeder channel, no bifurcation occurs. Although the modern channel has significant human influence, historical and geologic records indicate that the birdsfoot morphology was well established before large-scale human interference [*Fisk et al.*, 1954; *Kim et al.*, 2009a]. Recent numerical simulations that include cohesive sediment re-

[1]Department of Earth and Environmental Science, University of Pennsylvania, Philadelphia, Pennsylvania, USA.

0148-0227/10/2010JF001802

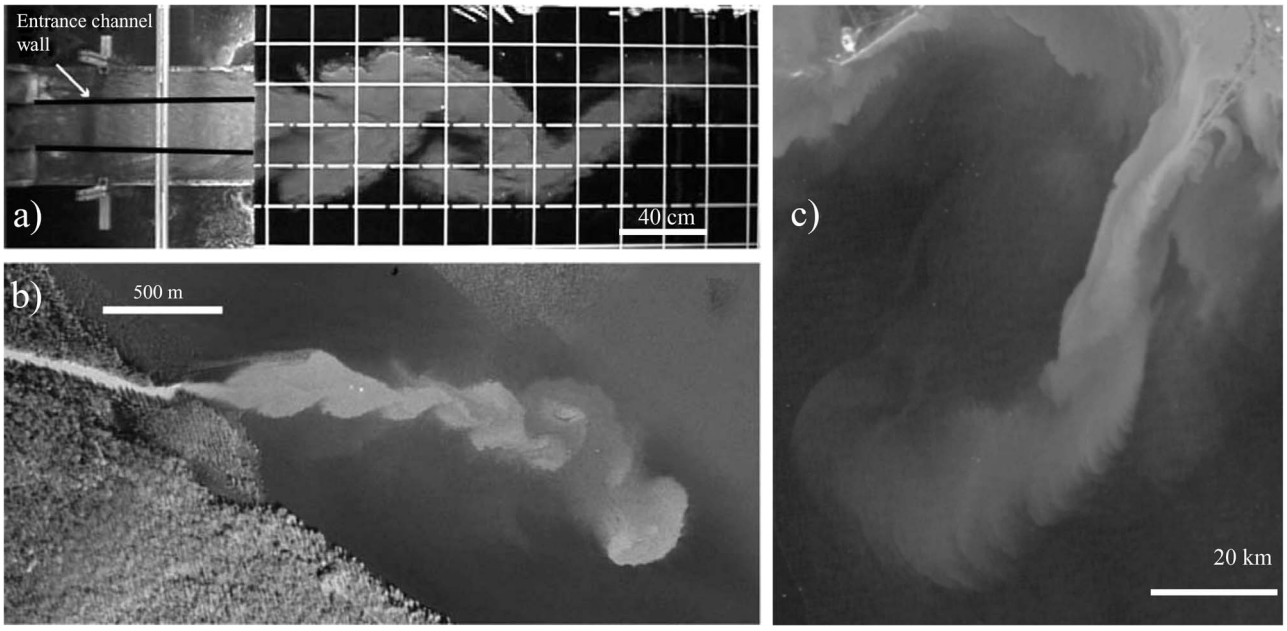

Figure 1. Different examples of jet plumes. (a) Experimental jet meander highlighted by fluorescent dye [from *Rowland et al.*, 2009a]. (b) Aerial photograph of a tie channel outlet discharging into an oxbow lake connected to the lower Mississippi River near Baton Rouge, LA, USA [from *Rowland et al.*, 2009a]. (c) *S*ediment laden plumes in northern Gulf of Mexico from the Southwest Pass of the Mississippi birdsfoot (credit: NASA Earth Observatory).

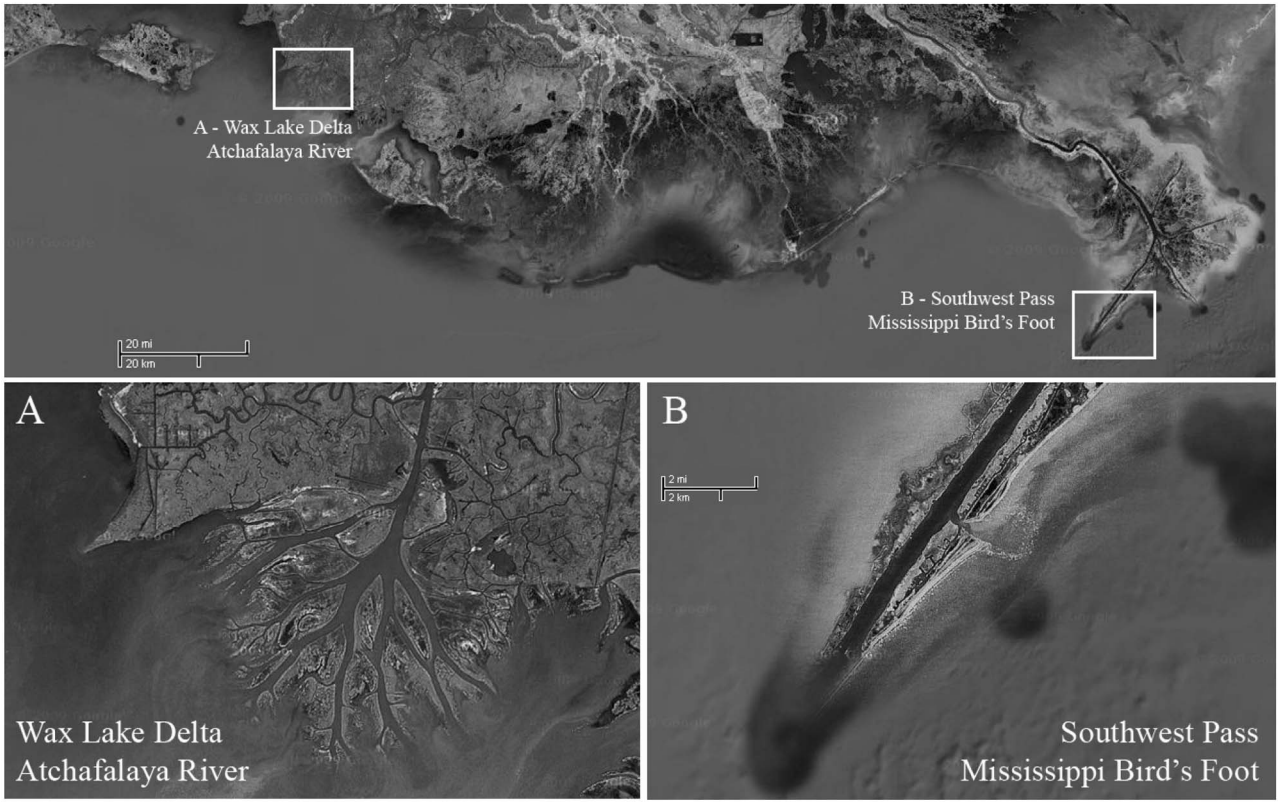

Figure 2. The lower Mississippi Delta and Louisiana coast, with the details of (a) Wax Lake Delta of the Atchafalaya River and (b) Southwest Pass of the Mississippi birdsfoot. Google Earth imagery ©Google Inc. Used with permission.

Figure 3. Aerial photograph of one of the tie channels studied by *Rowland* [2007], near Baton Rouge, LA, USA (color infrared orthophoto, SW quadrant of Angola quadrangle, LA, 2004 U.S. Geological Survey Digital Ortho Quarter Quadrangles (DOQQs) source: http://atlas.lsu.edu/). Asterisk and number sign represent the channel junction with the Mississippi River and the channel terminus at the Raccourci Old River oxbow lake, respectively. Arrow represents the Mississippi River flow direction.

produced the general birdsfoot shape [*Edmonds and Slingerland*, 2010], but at present we still lack a quantitative understanding of the conditions that give rise to bifurcating versus elongate channels. This hinders our ability to predict, for example, land-building patterns that would result from restoration activities involving diversions on the Mississippi and other deltas [*Parker and Sequeiros*, 2006; *Kim et al.*, 2009a].

[4] One common type of elongate channel seen in nature is tie channels, secondary channels that connect rivers to floodplain lakes [*Rowland*, 2007]. These remarkable features can prograde indefinitely without bifurcation (Figures 1 and 3) and, taking the length of channel (L) by its width (B) as a measure of elongation, they can reach $L/B \sim 80$ (Figure 3). Despite their diminutive size, tie channels bear a striking similarity to distributaries on the Balize lobe and in particular with the Southwest Pass which shows the same elongation ratio (Figure 2). Tie channels appear to us to be an end-member of the birdsfoot morphology, prompting us to seek similarity in the hydrodynamic and sediment transporting conditions between these systems. Recent field and experimental studies demonstrate that sediment transport in tie channels is almost entirely in suspension, resulting in rapid levee growth and progradation [*Rowland et al.*, 2009b]. It seems reasonable to suppose that suspended sediment and consequent levee growth at the river mouth is a necessary condition for elongate channels. Experiments demonstrate that cohesion is not necessary for subaqueous levee deposition [*Rowland*, 2007; *Rowland et al.*, 2009a], however it seems likely that cohesive sediments enhance this process [*Edmonds and Slingerland*, 2010].

[5] We hypothesize that elongate (nonbifurcating) channels form where levee growth is rapid compared to within-channel or mouth-bar depositions. Accordingly, in this paper we seek to determine the hydrodynamic and sediment transport conditions that lead to enhanced deposition at the margins of the river effluent jet. Since detailed measurements of flow and sediment transport at river mouths are limited, in this paper we will employ satellite observations of sea surface temperature and ocean color to examine the hydrodynamics and sediment concentration of river outflows. We observe a qualitative similarity between elongate channel jets and cold oceanic filaments [*Bignami et al.*, 2008], which are shallow veins of wind-sheared water having high potential vorticity and low lateral spreading (Figure 4). This similarity provides the basis for a new modeling approach, in which we adapt geophysical fluid dynamics theory from oceanography to describe river mouth jets. Recent tank experiments of river-mouth levee deposition by *Rowland* [2007] and *Rowland et al.* [2010] provide the main empirical motivation and constraints for our model.

[6] Our approach is based on the premise that sediment-laden river flows form a turbulent jet that expands and decelerates at rates that depend on initial hydrodynamic conditions [*Peckham*, 2008, and references therein] and frictional effects. Friction and lateral mixing processes extract the along-

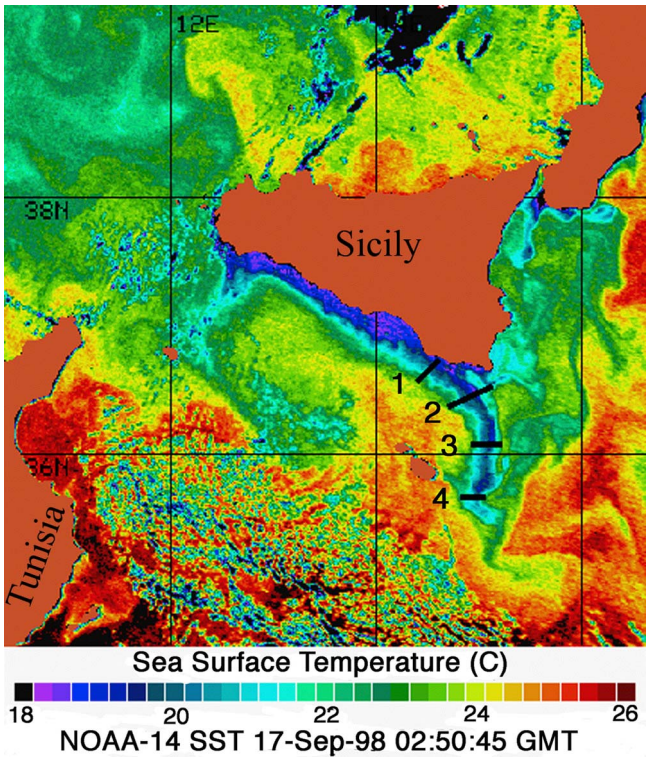

Figure 4. NOAA/AVHRR sea surface temperature (SST) image (NOAA 14 satellite) for 17 September 1998 of SE Sicily (Italy) shoreline, showing a cold filament entering the Ionian Sea. Numbers show the cross-sectional measurements of temperature contrasts between the core of the filament and the surrounding water: (1) 3.485°C, (2) 3.395°C, (3) 2.988°C, and (4) 2.20°C (courtesy of E. Salusti, 2009).

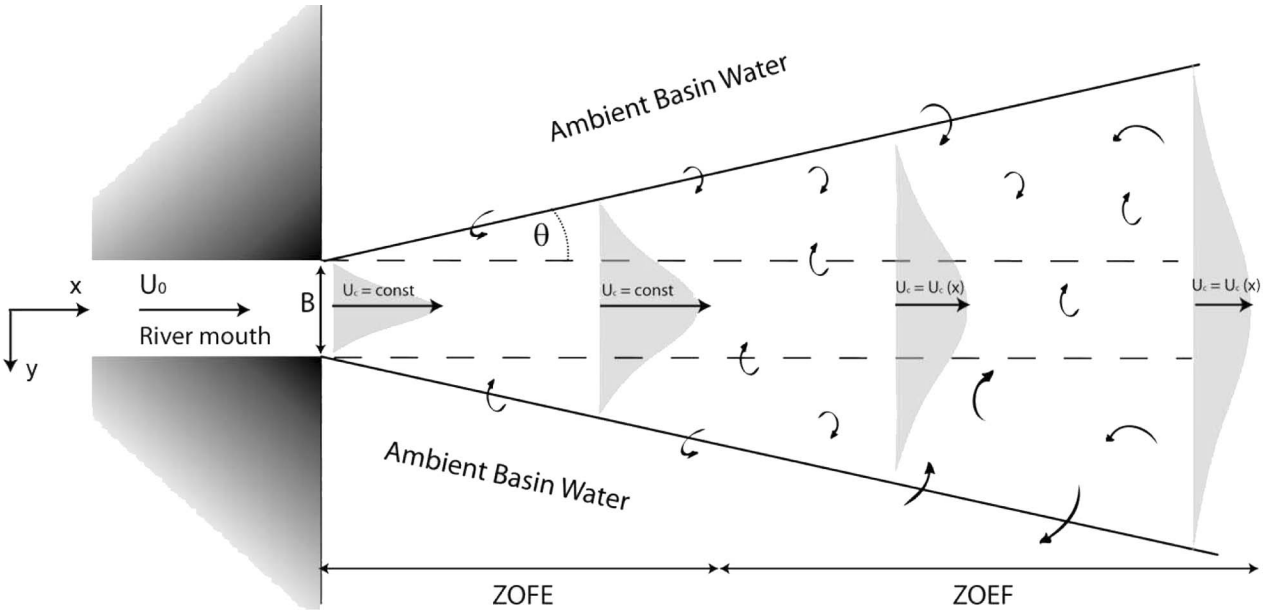

Figure 5. Schematic representation for spreading, diffusion, and deceleration of a typical confined wall jet. U_0 is the main flow velocity at the river mouth. Shaded areas indicate the Gaussian shape of the horizontal velocity profile, where the straight arrows represent the jet centerline velocity U_c. At the bottom, the Zone of Flow Establishment (ZOFE) and the Zone of Established Flow (ZOEF) are shown; within ZOFE $U_c = const$ whereas within the ZOEF $U_c = U_c\,(x) \equiv U_0\,(x/B)^{-\gamma}$, where γ is an experimental decay parameter. The spreading angle θ is related to the coefficient q (see text). Bent arrows represent the lateral entrainment/disentrainment with the ambient basin water and the fully turbulent regime experimentally recognized in the ZOEF [*Peckham*, 2008; *Rowland et al.*, 2009a].

flow mean kinetic energy, causing sediment deposition [*Wright*, 1977; *Edmonds and Slingerland*, 2007; *Peckham*, 2008]. The turbulent jet can be characterized in two dimensions as a horizontal Gaussian velocity profile that flattens and widens downstream due to shearing and lateral mixing at jet margins [*Albertson et al.*, 1950; *Abramovich*, 1963; *Schlichting*, 1968]. Following *Pedlosky* [1987], we derive the vorticity equation and characterize the hydrodynamic pattern of a planar jet in terms of vorticity. We then introduce a new kind of potential vorticity (PV hereafter) that incorporates sediment concentration. By means of the Ertel PV theorem [*Ertel*, 1942; *Pedlosky*, 1987], we derive a new equation for describing sedimentation patterns at the river mouth. The resultant PV model appears to explain key aspects of levee deposition and channel morphology, and is in reasonable agreement with experimental results [*Rowland*, 2007; *Rowland et al.*, 2009a]. Our theory predicts that high PV is a necessary condition for the creation of elongate channels such as the Mississippi birdsfoot. Synthesis of recently published field, laboratory and numerical studies confirms that PV is an important control on channel morphology. We conclude with suggestions for how the PV model could be used for designing water and sediment diversions to construct new delta lobes in threatened coastal areas [e.g., *Kim et al.*, 2009a].

2. Background in River Jet Dynamics

[7] Because river mouth sedimentation patterns are closely related to the characteristics of turbulent jet spreading, much research has focused on the hydrodynamics of river outflows [e.g., *Bates*, 1953; *Abramovich*, 1963; *Rajaratnam*, 1976; *Wright*, 1977; *Wang*, 1984; *Syvitski et al.*, 1998; *Peckham*, 2008, and references therein]. *Wright* [1977] was the first to directly relate different river mouth sedimentation patterns seen on deltas to fundamental hydrodynamic controls (Figure 5). Beginning with knowledge of classical jet theory [*Bates*, 1953; *Abramovich*, 1963], he qualitatively assessed the relative importance of frictional, inertial and buoyancy effects for controlling delta morphology. In particular, *Wright* [1977] introduced "inertia-dominated effluents," supercritical jets characterized by a Gaussian lateral velocity distribution, a high outflow velocity, a constant low spreading angle and weak streamwise velocity decay. These hydrodynamic conditions were thought to occur for deep channel outlets having little bed load transport. He proposed that the result of this flow configuration is a prograding, narrow lunate bar deposited in front of the channel mouth. "Friction-dominated effluents," characterized by a more moderate outflow jet velocity and rapid lateral expansion and deceleration, were thought to give rise to rapid deposition of a mouth bar in the channel centerline resulting in bifurcation. *Wright* [1977] suggested this kind of jet was associated with shallow channel outlets having high bed load. To provide an explanation for elongated channels *Wright* [1977] introduced "buoyant effluents," critical flows (Froude number ~1) characterized by strong stratification resulting from the salinity contrast between river outflows and the ocean, and by an intermediate flow velocity. He proposed that such buoyancy flows generate a secondary circulation able to

carry sediments from the centerline of the jet to the boundaries. The idea of buoyancy effluents as an explanation for elongated channels would appear to be refuted by the formation of such channels in freshwater lakes; nonetheless, Wright's ideas provided the framework for subsequent quantitative work.

[8] A significant advance in understanding river mouth sedimentation was made by *Edmonds and Slingerland* [2007], who used the Delft3D coupled hydrodynamic-morphodynamic model to simulate the processes of mouth-bar formation and levee growth resulting from an expanding sediment-laden jet. The three-dimensional conservation of momentum equations for unsteady, incompressible, turbulent flow introduced by *Edmonds and Slingerland* [2007], can be written in their general form as

$$\frac{\partial \vec{u}}{\partial t} + (\vec{u}\cdot\nabla)\vec{u} + 2\vec{\Omega}\times\vec{u} = -\frac{1}{\rho}\nabla p + \nabla\varphi + \frac{\vec{F}}{\rho}, \qquad (1)$$

where in a Cartesian frame, $\vec{u} = (u, v, w)$ is the velocity of the outflowing current, $2\vec{\Omega}\times\vec{u}$ is the Coriolis acceleration (m/s^2), Ω is the angular velocity of the frame of reference (i.e., the planetary vorticity, s^{-1}), p is the fluid pressure (N/m^2), ρ the density (kg/m^3), φ the force potential due to the body force (i.e., the gravity) and $\vec{F}$ the external force per unit volume (N/m^3).

[9] In particular, the Delft3D model used by *Edmonds and Slingerland* [2007] considered: the Coriolis acceleration in f plane approximation, namely $2\vec{\Omega}\times\vec{u} = (-fv, fu, 0)$; the potential field as $\nabla\varphi = (g_x, g_y, g_z)$; and the external force vector as $\vec{F} = \frac{\partial \tau_{xij}}{\partial x_j}$, where $x_i = (x, y, z)$ and τ_{xij} are the fluid shear stresses (N/m^2). The model also used a zero-divergent flow, namely $\nabla\cdot\vec{u} = 0$, and employed the following suspended sediment transport equation:

$$\frac{\partial c^i}{\partial t} + \nabla\cdot\left(\vec{u}c^i\right) - \frac{\partial\left(w_s^i\right)c^i}{\partial z} = \nabla\cdot\left[\left(\vec{k}_s\cdot\nabla\right)c^i\right], \qquad (2)$$

where c^i is the mass concentration of the ith sediment fraction (kg/m^3), w_s^i is the hindered sediment settling velocity of the ith sediment fraction (m/s) and $\vec{k}_s = (k_{sed}^x, k_{sed}^y, k_{sed}^z)$ represents the vector of the lateral (x, y) and vertical (z) sediment eddy diffusivity coefficients of the ith sediment fraction (m^2/s). These coefficients are somehow related to the diffusivity coefficient of the momentum $\vec{k} = (k^x, k^y, k^z)$. A full discussion on past efforts to determine the relation between these coefficient can be found by *Rowland* [2007].

[10] Under the range of conditions explored, the *Edmonds and Slingerland* [2007] simulations produced significant mouth-bar deposition resulting in formation of a bifurcating channel through the following sequence: (1) sediment flux divergence from jet deceleration leads to formation of a frontal bar, (2) suspended sediment deposition at jet margins builds levees that prograde basinward, leading to progradation of the frontal bar, and (3) vertical aggradation of the bar eventually produces a pressure gradient sufficient to cause divergence of flow around the bar. *Edmonds and Slingerland* [2007] quantitatively related bifurcation length to the initial width and depth of the parent channel, and also the initial velocity distribution and sediment grain size of the river jet at the channel mouth. Their results compare favorably to field observations of branching river deltas, but simulations did not produce elongated channels. In a more recent study [*Edmonds and Slingerland*, 2010], these authors added cohesive sediments to the Delft3D model and were able to simulate elongate channels, showing how variations in cohesion alone may force transition from a branching to elongate morphology.

[11] Recent laboratory tank experiments by *Rowland* [2007] and *Rowland et al.* [2009a] provide empirical constraints for flow and sediment transporting conditions associated with the formation of elongated channels. Their experiments were designed to mimic conditions of tie channels (Figures 1 and 3), which are narrow, deep channels transporting fully suspended sediment that is debouched as a shallow, wall-bounded plane jet [*Rowland et al.*, 2009a]. Sediment in their experiments was noncohesive. Measurements provided vertical and horizontal profiles for both fluid velocity and sediment concentration of the jet spreading into still ambient water (Figure 6). Results demonstrated the Gaussian self-similarity of the jet streamwise horizontal velocity, and also the oscillating behavior of $v(x,y)$ along the cross-stream direction due to lateral entrainment of ambient water (Figure 6). Outflows produced focused sedimentation at jet margins with very limited deposition along the jet centerline, leading to construction of subaqueous levees but not frontal bars [*Rowland*, 2007]. Thus, conditions likely corresponded to the transport regime under which elongate channels form.

[12] Experimental jets exhibited robust behavior: the horizontal velocity profile was well described by the classical Gaussian shape [*Albertson et al.*, 1950; *Abramovich*, 1963; *Wang*, 1984; *Peckham* 2008], which decayed downstream in a self-similar manner as a result of friction and lateral entrainment:

$$u(x,y,z) = u_c(x,z)G(y), \qquad (3a)$$

$$v(x,y) = E_w(u)u_c(x). \qquad (3b)$$

In equations (3a) and (3b) u_c is the jet centerline velocity, $G(y)$ is a Gaussian similarity function [*Wang*, 1984; *Peckham*, 2008; *Rowland et al.*, 2009a] which provides the cross-stream structure of the jet; and E_w is an entrainment function that describes lateral mixing and is dependent on jet velocity [*Ellison and Turner*, 1959; *Turner*, 1986]. As postulated by *Wright* [1977], *Rowland*'s [2007] experiments show that both lateral jet spreading and sediment transport to the margins are driven by the same process: shearing and entrainment of ambient water at the jet margins drives the lateral transfer of mass and momentum.

[13] A specific presentation of all factors in equations (3a) and (3b) is provided by *Peckham* [2008] who lists different analytic models for jet solutions. By quantifying these functions, and in particular $u_c(x)$, *Rowland et al.* [2009a] provided strong experimental validation of the self-similarity approach. They compared empirical results with well-established analytic formulations and data from planar jets

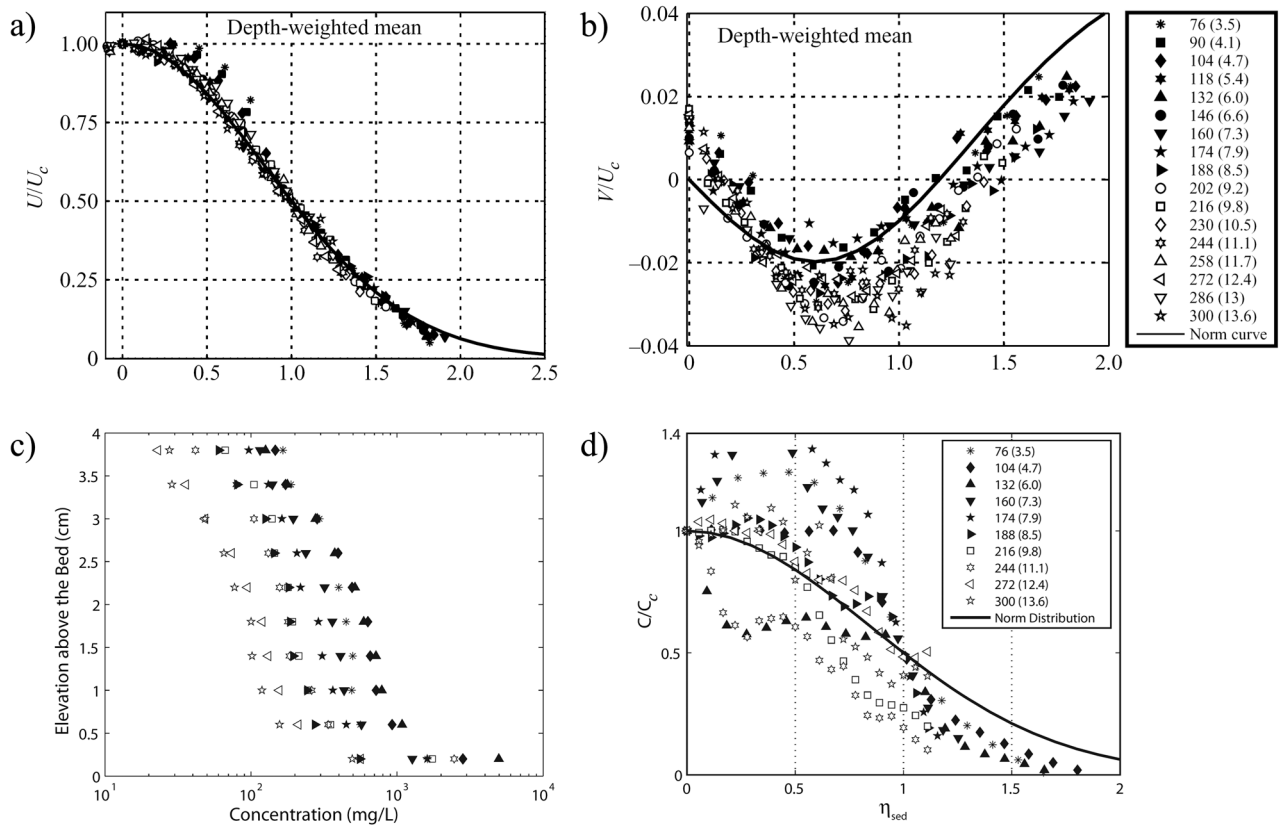

Figure 6. Data plots from the *Rowland* [2007] and *Rowland et al.* [2009a] experiments for a wall-bounded plane jet study: (a) horizontal profile of the normalized depth-weighted mean streamwise velocity, (b) horizontal profile of the normalized depth-weighted mean cross-stream velocity, by the normalized cross-stream coordinate $\eta = y/b(x)$, (c) vertical suspended sediment concentration profiles, (d) normalized depth averaged suspended sediment concentrations, by the normalized cross-stream coordinate $\eta_{sed} = y/b_s(x)$. Solid and open symbols correspond to measurements within the ZOFE and the ZOEF, respectively. The solid lines in Figures 6a and 6b represent the similarity profiles defined by equations (4) and (5), respectively. Numbers in the legend represent distance in centimeters from the outlet and the normalized distances (x/B) are in parentheses. In Figures 6a and 6b the streamwise and cross-stream velocities are normalized by the local centerline streamwise velocity (U_c), and the lateral position (y) is normalized by the half-width $b(x)$, defined as the point where downstreamflow velocity reaches half the value of U_c [*Rowland et al.*, 2009a]. In Figure 6d the concentrations are normalized by the local centerline concentration (C_c), and the lateral position (y) is normalized by the concentration half width $b(x)$, defined as the point where downstream concentration reaches half the value of C_c [*Rowland*, 2007].

provided by several authors [*Bates*, 1953; *Schlichting*, 1968; *Tennekes and Lumley*, 1972; *Wang*, 1984; *Giger et al.*, 1991; *Dracos et al.*, 1992]. Inertia-dominated jets are supposed to maintain a fairly constant centerline velocity u_c for some distance basinward of the channel mouth [*Albertson et al.*, 1950; *Rowland*, 2007; *Peckham*, 2008]. The length of this "Zone Of Flow Establishment" (ZOFE, Figure 5) has been reported as being 4 to 6 channel widths [*Albertson et al.*, 1950; *Tennekes and Lumley*, 1972].

[14] In the outer zone, called "Zone Of Established Flow" (ZOEF, Figure 5), u_c decays in a self similar manner due to lateral mixing and frictional effects. *Rowland et al.* [2009a] confirmed *Albertson et al.*'s [1950] solutions for the 2-D turbulent jet model in this outer zone. The depth-averaged functions for equations (3a) and (3b) in the ZOEF can be written as [*Rowland et al.*, 2009a; *Peckham*, 2008]

$$U(x,y) = U_c(x)\exp\left(-\left(\frac{\sigma y}{b(x)}\right)^2\right) \equiv U_0\left(\frac{x}{B}\right)^{-\gamma}\exp\left(-\left(\frac{\sigma y}{b(x)}\right)^2\right), \quad (4)$$

$$V(x,y) = U_c(x)q\left(\frac{\sigma y}{b(x)}\exp\left(-\left(\frac{\sigma y}{b(x)}\right)^2\right) - \frac{\sqrt{\pi}}{4}erf\left(\frac{\sigma y}{b(x)}\right)\right), \quad (5)$$

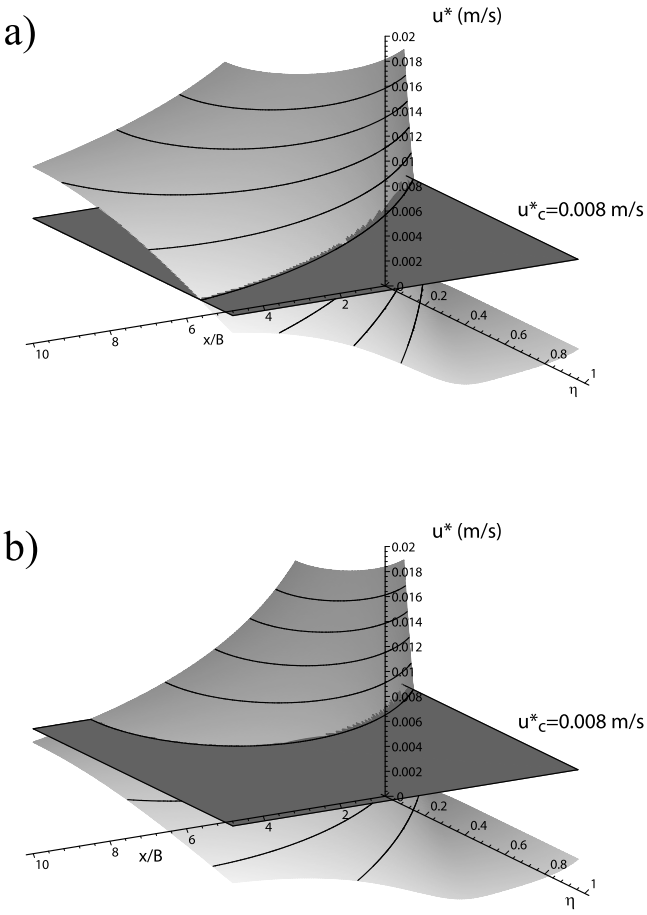

Figure 7. Shear velocities u^* (m/s) profiles along both the streamwise (x/B) and cross-stream ($\eta = y/b(x)$, where $b(x) = qx$) normalized distances, calculated using equations (4) and (5), with $C_d = 0.002$, $q = 0.1$ and the streamwise decay rates (a) $\gamma = 0.5$ and (b) $\gamma = 0.7$. The darker horizontal surface indicates the critical shear velocities needed to entrain the sediment type with $u_c^* = 0.008$ m/s into suspension, corresponding to a specific gravity of 1.2 and median grain size of 350 microns [*Rowland*, 2007]. The intersection between the two surfaces marks the deposition (darker surface higher than light surface) and suspension (light surface higher than darker surface) regions; higher decay rate ($\gamma = 0.7$, Figure 7b) allows frontal deposition at the river mouth after a short distance.

where U(x, y) and V(x, y) indicate depth-averaged values of $u(x, y, z)$ and $v(x, y, z)$, respectively; σ is an experimental factor, and $erf(t) = \frac{2}{\sqrt{\pi}} \int_{-\infty}^{t} \exp(-t'^2)dt'$. In equations (4) and (5) $U_c\,(x) = U_0\,(\frac{x}{B})^{-\gamma}$ represents the streamwise decay of the depth-averaged jet centerline velocity; γ and q are constants that can be related to the decay rate of the streamwise velocity due to bed friction and to the lateral spreading due to water entrainment, respectively (Figure 5). *Giger et al.* [1991] argued that the reduction in lateral entrainment (q) due to bed friction would offset increased spreading due to the increased rate in velocity reduction (γ), and hence that the spreading rate of a frictional jet would not differ from one in the absence of bed friction.

[15] The lateral position (y) in equations (4) and (5) is normalized by the half-width $b(x)$ of the Gaussian shape, defined as the point where down stream flow velocity reaches half the value of U_c [*Rowland et al.*, 2009a]. Theory and experiments tightly constrain the value $\gamma \approx 0.5$ [*Peckham*, 2008; *Rowland et al.*, 2009a], while $b(x) \sim qx$, where $q \approx 0.1$ is empirically determined [*Rowland et al.*, 2009a].

[16] *Rowland et al.* [2009a], confirming observations of *Bates* [1953], recognized the presence of a transitional zone between the ZOFE and the ZOEF where U_c decreases but not at the rate of the ZOEF (the observed rate was $\gamma \approx 0.15$) and a condition of self-similar Gaussian velocity distributions has not developed. The onset of ZOEF did not occur until ~8 outlet widths downstream of the outlet. The flow conditions and channel geometries selected by *Rowland et al.* [2009a], which are more representative of natural tie channels (Figures 1 and 3), therefore form more coherent jets that may penetrate large distances without significant mixing.

[17] *Rowland et al.* [2010] also showed that the spatial distribution of horizontal velocities is reflected in the distribution of boundary shear stresses. From equations (4) and (5), shear velocity along the ZOEF and the inner transitional zone can be obtained using the formulation $(u^*)^2 = C_d\,(U^2 + V^2)$, where C_d is a mean coefficient of friction (Figure 7). Although in a different analysis *Rowland et al.* [2009a] suggest that the distribution of turbulent stresses is also important, the time-averaged approach is a reasonable first step for an analytical approach. By comparing measured shear stresses to the critical shear stress required for entrainment of grains of various sizes, one can define zones of deposition that compare satisfactorily to actual sedimentation patterns (Figure 7). These results emphasize how the downstream evolution of the Gaussian horizontal velocity profile controls deposition and resuspension of sediments, a point that is reinforced by the results of *Rowland et al.* [2010] who found a good correspondence between measured fluid velocity and sediment concentration patterns in the ZOFE and in the transition zone between the ZOFE and the ZOEF. Indeed, in this zone, where sediment deposition at the lateral boundaries occurs and no momentum is lost at the jet centerline, the Gaussian shape must be narrower and sharper [*Peckham*, 2008].

3. Vorticity Model

[18] We hypothesize that elongate channels grow from focused levee deposition occurring at the inner stage of the jet, namely in the ZOFE and within the transition zone identified by *Bates* [1953] and *Rowland et al.* [2009a]. As shown in Figure 7, the general downstream evolution of the flow is strongly related to deposition along the jet margins, where we define deposition zones as locations where the shear stress is smaller than the critical shear stress. Therefore, a crucial step is to establish a general framework for describing the downstream evolution of the velocity pattern from the initial conditions at the river outlet (Figure 5). Let $\vec{\omega}$ be the vorticity of the jet, defined as $\vec{\omega} = \nabla \times \vec{u}$. The vertical component of the jet vorticity (ζ) is given by

$$\zeta(x, y, z) = \partial_x v - \partial_y u. \tag{6}$$

[19] While $\vec{\omega}$ gives the general internal rotation of the fluid, this ζ provides a more intuitive definition of vorticity,

Table 1. Bulk Values of Channel Width (B), Depth (h), Velocity at the Channel Outlet (U_0), and Suspended Sediment Concentration (C) for All Study Examples[a]

	Wax Lake	Numerical Runs	Southwest Pass	Tie Channels	Experimental Runs
B (m)	4×10^2	10^2–10^3	3×10^2	10–50	2.5×10^{-1}
h (m)	20	5–20	15	2–10	5×10^{-2}
U_0 (ms^{-1})	0.5	1–3	1.5	1–2	0.5
C (mgl^{-1})	150	200	100	200–600	500

[a]Wax Lake [*Myint and Walker*, 2002; *Buttles et al.*, 2007], numerical runs [*Edmonds and Slingerland*, 2007], Southwest Pass of the Mississippi River birdsfoot [from *Myint and Walker*, 2002; U.S. Army Corps Engineers, http://www.mvn.usace.army.mil], tie channels [*Rowland*, 2007], and experimental runs [*Rowland*, 2007; *Rowland et al.*, 2009a].

which describes the horizontal lateral spreading and shearing of the flow: the magnitude of ζ can be associated to the spinning of a paddle wheel that lies on the horizontal plane of the flow [*Holton*, 1992]. ζ may not be the main component of vorticity in shallow water systems: generally ζ is smaller than the cross-stream vorticity component related to the no-slip condition, that is $\psi = -(\partial_x w - \partial_z u) \approx \partial_z u$ (Table 1). This is particularly true for the ZOFE and for the following transition zone, but *Rowland et al.* [2009a] show that in the ZOEF the vertical gradient in streamwise velocity ($\partial_z u$) approaches zero and the flow is largely two-dimensional. From a physical point of view, ψ represents rotation in the vertical plane of the flow.

[20] Therefore, as pointed out by *Peckham* [2008], ζ is a useful tool to represent equations (3a) and (3b) in a more compact form, and as discussed above, horizontal velocity patterns play a fundamental role in sediment dynamics of jets (Figure 7). The horizontal velocity pattern observed by *Rowland et al.* [2009a] within the transition zone and the ZOEF, and described by equations (4) and (5), can be expressed in terms of ζ for different centerline velocity decay rates γ (Figure 8). From a vorticity analysis, one can observe that jets with a low decay rate γ show a higher vorticity (Figures 8a and 8b), a feature that confirms the correspondence between high vorticity and pronounced Gaussian shape of the horizontal velocity profile. We remark that our further vorticity analysis does not depend on the assumption of a Gaussian jet shape as in equations (3a) and (3b). Rather, we aim to demonstrate that well-accepted descriptions of horizontal velocity patterns such as equations (3a) and (3b) may be described by means of vorticity alone.

[21] We can compact the three components of the Navier-Stokes equations into one equation capable of describing the spatial variation of vorticity. Following *Pedlosky* [1987], the vector identity $(\vec{u} \cdot \nabla)\,\vec{u} = \vec{\omega} \times \vec{u} + \nabla\frac{|u|^2}{2}$, allows us to write the generalized three-dimensional conservation of momentum equation (1) as

$$\frac{\partial \vec{u}}{\partial t} + \left(2\vec{\Omega} + \vec{\omega}\right) \times \vec{u} = -\frac{1}{\rho}\nabla p + \nabla\left(\phi - \frac{|u|^2}{2}\right) + \frac{\vec{F}}{\rho}. \quad (7)$$

Taking the curl of (7) and recalling that $\nabla \times \nabla a = 0$, one obtains an equation for the vorticity:

$$\frac{\partial \vec{\omega}}{\partial t} + \nabla \times \left\{\left(2\vec{\Omega} + \vec{\omega}\right) \times \vec{u}\right\} = \frac{\nabla\rho \times \nabla p}{\rho^2} + \nabla \times \left(\frac{\vec{F}}{\rho}\right). \quad (8)$$

Using the relation [*Pedlosky*, 1987],

$$\nabla \times \left\{\left(2\vec{\Omega} + \vec{\omega}\right) \times \vec{u}\right\} = \left(2\vec{\Omega} + \vec{\omega}\right)\nabla \cdot \vec{u} + (\vec{u} \cdot \nabla)\left(2\vec{\Omega} + \vec{\omega}\right) - \left(2\vec{\Omega} + \vec{\omega}\right) \cdot \nabla\vec{u}, \quad (9)$$

and the requirement that absolute vorticity $\vec{\omega}_a = 2\,\vec{\Omega} + \vec{\omega}$ has zero divergence, the combination of (8) and (9) produces

$$\frac{d\vec{\omega}}{dt} = \left(2\vec{\Omega} + \vec{\omega}\right) \cdot \nabla\vec{u} - \left(2\vec{\Omega} + \vec{\omega}\right)\nabla \cdot \vec{u} + \frac{\nabla\rho \times \nabla p}{\rho^2} + \nabla \times \left(\frac{\vec{F}}{\rho}\right), \quad (10)$$

the well known vorticity equation. The first term on the right-hand side, somehow related to the gradient of each velocity component of the flow, represents the contribution of shearing of velocity to the rate of change of vorticity. The second term demonstrates that the convergence(divergence) of the flow, i.e., $\nabla \cdot \vec{u}$, will increase(decrease) its vorticity, a rather intuitive feature if we consider that vorticity increases as the cross-sectional area of the stream tube decreases.

[22] The third term is related to baroclinic effects that may occur at the interface between the river jet and seawater [*Pedlosky*, 1987]. For our purposes, the fourth term plays the most significant role since it is related to the bottom and lateral boundary shear stresses. Therefore it constitutes the main sink of vorticity of the system: as the bed friction increases, the centerline velocity will decrease more rapidly and hence the vorticity will decrease more rapidly (Figures 7 and 8) and therefore centerline deposition will increase.

[23] In a shallow water jet, where vertical motion can be neglected and the flow is largely two-dimensional (i.e., $\vec{u} = (u, v, 0)$ and $\frac{\partial \vec{u}}{\partial z} = 0$), the vertical component of equation (10) can be easily obtained by applying the cross derivative to the horizontal component of the Navier-Stokes equation, resulting in the simplified expression

$$\frac{\partial \zeta}{\partial t} + (\nabla \cdot \vec{u})\zeta + (\zeta + f)(\nabla \cdot \vec{u}) = \nabla \times \left(\frac{\vec{F}}{\rho}\right). \quad (11)$$

[24] This expression (11) for vertical vorticity may be used to describe the relevant spatial structure of a turbulent planar jet once appropriate boundary conditions are applied. Physically, equation (11) represents the spatiotemporal evolution of the horizontal velocity profile (i.e., the Gaussian profile) of the jet; its centerline velocity, spreading and lateral shearing.

4. Potential Vorticity Theorem Applied to a Sediment-Laden Jet

[25] The vorticity approach is a powerful hydrodynamic formulation, however it does not yet include any description of suspended sediments, which is essential for predicting patterns of deposition at river mouths. In this section we introduce a new kind of potential vorticity (PV) that includes the suspended sediment concentration pattern. Through use of the *Ertel* [1942] PV theorem, and consideration of sediment mass conservation, we derive a new

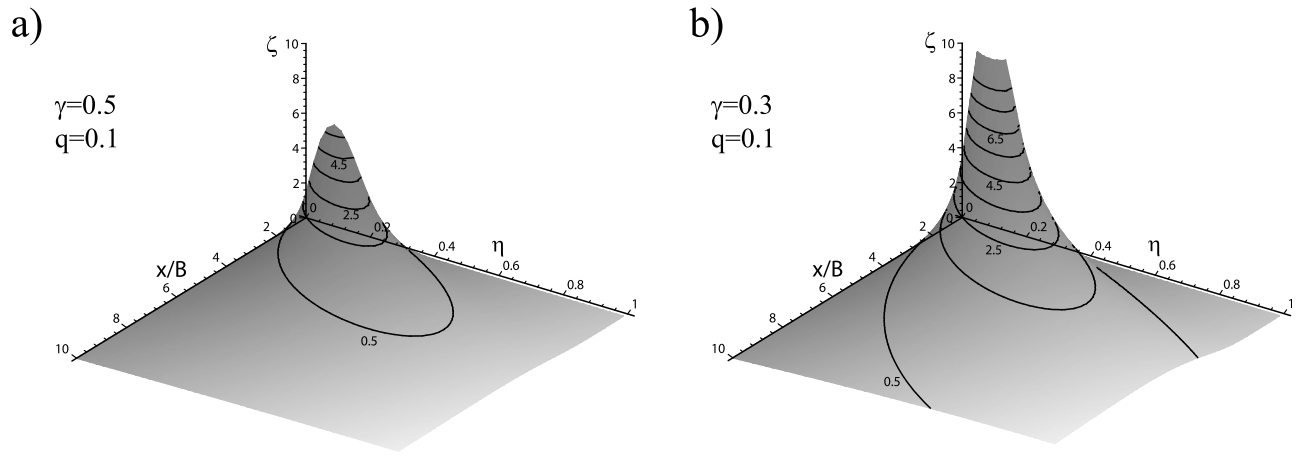

Figure 8. Flow vorticity, ζ (s^{-1}) profile along both the streamwise (x/B) and cross-stream ($\eta = y/b(x)$, where $b(x) = qx$) normalized distances, calculated using the equations (6), (4), and (5) with (a) $\gamma = 0.5$ and (b) $\gamma = 0.3$, for $q = 0.1$. Comparison between Figures 8a and 8b shows the increase of ζ for decreasing the streamwise decay rate γ, with a constant lateral spreading.

expression that may be used to describe spatial patterns of deposition associated with sediment-laden river jets. Because the Ertel theorem also includes the conservation of mass equation for the fluid, it is the most general analytical framework for studying sediment-laden river jets. More generally, this novel method extends the PV approach beyond its classical applications in meteorology and physical oceanography.

[26] Use of PV requires introduction of an arbitrary scalar quantity (λ), and thus its variability in space and time. The general definition of PV is

$$\Pi_\lambda = \frac{\vec{\omega}_a}{\rho} \cdot \nabla\lambda, \tag{12}$$

where $\vec{\omega}_a = \vec{\omega} + 2\vec{\Omega}$ is the absolute vorticity. Classical choices for λ in meteorology and physical oceanography are: the thickness of the water/air column; the potential temperature; or the potential density of the water/air. The Ertel PV theorem provides a powerful aid for describing the physics of a wide variety of motions, depending on the choice of lambda [*Gill*, 1982; *Pedlosky*, 1987; *Muller*, 1995]. Here we make a novel selection for the scalar, $\lambda = c$, where $c = c(x, y, z, t)$ represents the suspended sediment concentration within the river jet. We are not aware of any study that has cast PV in terms of sediment concentration, however it seems a natural choice for studying sediment transport dynamics.

[27] Following *Pedlosky* [1987], we demonstrate the derivation of PV (12) by means of the *Ertel* [1942] theorem, which is based on the vorticity equation (10) and the continuity equation

$$\nabla \cdot \vec{u} = -\frac{1}{\rho}\frac{d\rho}{dt}, \tag{13}$$

which represents a more general relation than the divergence-free assumption used by *Edmonds and Slingerland* [2007].

[28] Recognizing that $\frac{d\vec{\omega}_a}{dt} = \frac{d\vec{\omega}}{dt}$, equation (13) allows us to recast equation (10) as

$$\frac{d\vec{\omega}_a}{dt} = \vec{\omega}_a \cdot \nabla\vec{u} + \frac{\vec{\omega}_a}{\rho}\frac{d\rho}{dt} + \frac{\nabla\rho \times \nabla p}{\rho^2} + \nabla \times \left(\frac{\vec{F}}{\rho}\right). \tag{14}$$

Considering the equality $\frac{d}{dt}\left(\frac{\vec{\omega}_a}{\rho}\right) = \frac{1}{\rho}\frac{d\vec{\omega}_a}{dt} - \frac{\vec{\omega}_a}{\rho^2}\frac{d\rho}{dt}$ allows equation (14) to be written in a more compact form:

$$\frac{d}{dt}\left(\frac{\vec{\omega}_a}{\rho}\right) = \left(\frac{\vec{\omega}_a}{\rho} \cdot \nabla\right)\vec{u} + \frac{\nabla\rho \times \nabla p}{\rho^3} + \frac{1}{\rho}\nabla \times \left(\frac{\vec{F}}{\rho}\right). \tag{15}$$

[29] We assume that suspended sediment concentration within the jet can be considered as a scalar fluid property that is not materially conserved, such that

$$\frac{dc}{dt} = \Psi, \tag{16}$$

where Ψ is a source/sink term for c, and thus is related to the ability of the system to erode and/or deposit sediments at the boundaries. Introducing this scalar quantity, one can take the dot product of ∇c and equation (15), obtaining

$$\nabla c \cdot \frac{d}{dt}\left(\frac{\vec{\omega}_a}{\rho}\right) = \nabla c \cdot \left[\left(\frac{\vec{\omega}_a}{\rho} \cdot \nabla\right)\vec{u}\right] + \nabla c \cdot \frac{\nabla\rho \times \nabla p}{\rho^3} + \frac{\nabla c}{\rho} \cdot \left[\nabla \times \left(\frac{\vec{F}}{\rho}\right)\right], \tag{17}$$

which after some tedious algebra, gives

$$\frac{d}{dt}\left(\frac{\vec{\omega}_a}{\rho} \cdot \nabla c\right) = \frac{\vec{\omega}_a}{\rho} \cdot \nabla\Psi + \nabla c \cdot \frac{\nabla\rho \times \nabla p}{\rho^3} + \frac{\nabla c}{\rho} \cdot \left[\nabla \times \left(\frac{\vec{F}}{\rho}\right)\right]. \tag{18}$$

Equation (18) is known as the *Ertel* [1942] PV theorem and it expresses the temporal and spatial variations of PV,

namely $\Pi_c = \frac{\vec{\omega}_a}{\rho} \cdot \nabla c$, in terms of sediment mass conservation, baroclinic effects and frictional forces.

[30] Assuming that the vertical component of the velocity as well as any vertical variations of the cross stream velocity are negligible (i.e., w, $\frac{\partial v}{\partial z} \approx 0$), the scalar product in the definition of Π_c can be explicitly written as

$$\Pi_c = \frac{1}{\rho}\left(\frac{\partial u}{\partial z}\frac{\partial c}{\partial y} + (\zeta + f)\frac{\partial c}{\partial z}\right). \tag{19}$$

It is worth noting that the definition of PV in equation (19) collects all the key features of a spreading jet, where the vertical shear velocity and the Gaussian shape of the horizontal velocity profile (as well as its spatial evolution) are coupled with the horizontal and vertical distribution of suspended sediment.

[31] Let us now reasonably assume that $\nabla c \cdot \nabla \rho \times \nabla p = 0$ for a planar jet, since the density of a sediment-laden river outflow has only a very mild dependence on temperature and salinity and thus $\rho = \rho(c, p)$; this means that the baroclinic effect can be neglected. We also assume that the resistive forces act principally along the horizontal axes, which means that the curl of the forces lies along the vertical axis. It follows that equation (18) may be written in a more compact form:

$$\frac{d}{dt}\Pi_c = \frac{\vec{\omega}_a}{\rho} \cdot \nabla \Psi + \frac{1}{\rho}\nabla c \cdot \left[\nabla \times \left(\frac{\vec{F}}{\rho}\right)\right]. \tag{20}$$

Equation (20) represents a very useful formulation of the *Ertel* [1942] PV Theorem, able to describe a sediment-laden river jet system affected by external forces due to both lateral and bottom shear stresses as well as depositional/erosive effects (if $\Psi \neq 0$).

[32] We now consider in more detail the sediment mass conservation term in equation (20), namely the first term on the right-hand side, which may constitute a source/sink term of PV. The material derivative for suspended sediment concentration can be expressed as $\Psi = E - D$, where E and D are erosion and deposition functions, respectively, and are typically empirically determined [*Parker*, 1978]. One generic approach is to consider Ψ as the result of the (upward) diffusivity of sediments and the (downward) settling of sediments at terminal fall velocity (w_s). Therefore, sediment mass conservation (2) for a single grain-size population can be generally expressed in its Eulerian form [*Necker et al.* 2002]:

$$\Psi = \frac{dc}{dt} = \nabla \cdot \left[\left(\vec{k}_s \cdot \nabla\right)_b c\right] - w_s\left(\frac{\partial c}{\partial z}\right)_b, \tag{21}$$

where the subscript b indicates that the derivatives are evaluated at the bottom. Calling now $d = (\vec{k}_s \cdot \nabla)_b c$, one obtains

$$\begin{aligned}\nabla\Psi &= \nabla\left(\nabla \cdot \vec{d}\right) - v_s \nabla\left(\frac{\partial c}{\partial z}\right)_b \\ &\equiv \nabla^2 \vec{d} + \nabla \times \left(\nabla \times \vec{d}\right) - w_s \nabla\left(\frac{\partial c}{\partial z}\right)_b,\end{aligned} \tag{22}$$

which describes the sediment mass conservation term in equation (20) as a "gradient of divergence" operating on the vector $\vec{d}$, minus the gradient of the downward sediment flux. In this way equation (20) represents a general model, which must be closed using the following: (1) an empirical determination of the spatial distribution of the suspended sediment concentration (the vector $\vec{d}$) and (2) knowledge of the settling velocity (w_s) and external forces. As discussed later on, the sediment mass conservation term in (20), and thus $\nabla\Psi$, will be neglected since we assume that the loss of sediment close to the river mouth does not affect the hydrodynamics of the jet.

5. Physical Approximations and Closure of the Model

[33] Our new definition of Π_c in equation (19) can be seen as a general variable that incorporates all of the key hydrodynamic and suspended sediment features. For flow and channel geometry conditions of jet experiments, where focused levee deposition occurred [*Rowland*, 2007; *Rowland et al.*, 2009a, 2010], and for field cases emanating from elongate channels, planetary vorticity ($f \approx 10^{-4}\ s^{-1}$) is significantly smaller than jet vertical vorticity. From Tables 1 and 2 one can obtain

$$\frac{\partial u}{\partial z}\frac{\partial c}{\partial y} + (\zeta + f)\frac{\partial c}{\partial z} \approx \frac{\partial u}{\partial z}\frac{\partial c}{\partial y} + \zeta\frac{\partial c}{\partial z} \approx 2\frac{\Delta U}{\Delta h}\frac{\Delta c}{\Delta B}, \tag{23}$$

where $\zeta \approx \frac{\Delta U}{\Delta B}$, $\frac{\partial u}{\partial z} \approx \frac{\Delta U}{\Delta h}$, and $\frac{\partial c}{\partial y} \approx \frac{\Delta c}{\Delta B}$. The scaling in equation (23) stresses that all of the derivatives in equation (20) may play a role in the PV dynamics. Indeed, for the systems we consider (Table 2), $\zeta\frac{\partial c}{\partial z}$ is 1–10 times larger than $\frac{\partial u}{\partial z}\frac{\partial c}{\partial y}$, suggesting that there could be a spot in parameter space (U, C, h) where lateral shear (ζ), vertical shear ($\frac{\partial u}{\partial z}$), and suspended sediment lateral and vertical gradients ($\frac{\partial c}{\partial z}$, $\frac{\partial c}{\partial y}$) combine together to promote elongation. However, as observed in *Rowland*'s [2007] experiments, within the ZOEF (i.e., where the jet has been experimentally observed as a two-dimensional flow) the predominant source of PV is mainly given by the lateral shearing and the vertical distribution of suspended sediment concentration.

[34] A scale analysis (Table 1) shows that the mass conservation term (20) may be further simplified as

$$\nabla\Psi = \left[0, 0, \frac{\partial}{\partial z}\left(\frac{\partial}{\partial z}k_{sed}^z\left(\frac{\partial c}{\partial z}\right)_b - w_s\left(\frac{\partial c}{\partial z}\right)_b\right)\right], \tag{24}$$

which tells us that if the upward flux of sediment due to turbulence is balanced by the downward flux, namely $\frac{\partial}{\partial z}k_{sed}^z\left(\frac{\partial c}{\partial z}\right)_b \approx w_s\left(\frac{\partial c}{\partial z}\right)_b$, then

$$\nabla\Psi \approx 0. \tag{25}$$

[35] Since the term $\frac{\vec{\omega}_a}{\rho} \cdot \nabla\Psi$ in equation (20) is actually a source/sink term for PV, equation (25) suggests that when exchange of sediments between the jet and the boundaries can be neglected, PV changes must be governed by frictional effects only. In a jet forming elongate channels, experimental results demonstrate that the delivery of sediments toward the jet margins is related to the cross-stream sediment diffusion term, $\frac{\partial}{\partial y}\left(k_{sed}^z\frac{\partial c}{\partial y}\right)$ [*Rowland*, 2007]. For these systems it is reasonable to assume that the amount of sediment loss from deposition is significantly lower than for

Table 2. Bulk Values of Vertical ($\frac{\Delta C}{\Delta h}$) and Horizontal ($\frac{\Delta C}{\Delta B}$) Profiles for Suspended Sediment Concentration, Vertical Profile for Streamwise Velocity ($\frac{\Delta U}{\Delta h}$), Vorticity ($\zeta$), and PV ($\Pi_c$) as Obtained From Table 1

	Wax Lake	Numerical Runs	Southwest Pass	Tie Channels	Experimental Runs
$\frac{\Delta C}{\Delta h}$ (mg/(ml))	10	10	10	50	10^2
$\frac{\Delta C}{\Delta B}$ (mg/(ml))	10^{-1}	5×10^{-2}	10^{-1}	5	10
$\frac{\Delta U}{\Delta h}$ (s^{-1})	5×10^{-2}	5×10^{-2}	10^{-1}	10^{-1}	5
ζ (s^{-1})	5×10^{-4}	10^{-3}	5×10^{-3}	5×10^{-2}	1
$\rho\Pi_c$ (mg/(mls))	5×10^{-3}	10^{-2}	5×10^{-2}	1	10^2

jet systems forming frontal bars, and thus bifurcating channels, where the bar formation may represent a loss of jet momentum [*Rowland*, 2007; *Edmonds and Slingerland*, 2007]. The physical implication for jets forming elongate channels is that one can approximately assume that $\nabla\Psi \approx 0$, and therefore that frictional effects dominate the downstream decrease in PV. We however remark that an analytic shape for $\nabla\Psi$ can be of crucial importance for further theoretical developments since it may constitute a conspicuous sink term of PV.

[36] Finally, model closure requires a relation for the frictional (last) term in equation (20). Assuming that the resistive forces act along the horizontal axes only, a realistic nonlinear friction relation takes the form

$$\vec{F} = \frac{-K_{(n,m)}\rho}{h^m}|\vec{u}|^n\vec{u}, \tag{26}$$

where n and m are integers and $K_{n,m}$ is an empirical coefficient. With the aid of equation (26), for $n = 1$ and for small v, the frictional term in (20) can be written as

$$\left[\nabla \times \frac{\vec{F}}{\rho}\right]_z \approx -2K\frac{u}{h}\zeta \text{ and } \left[\nabla \times \frac{\vec{F}}{\rho}\right]_y \approx -2K\frac{u}{h}\frac{\partial u}{\partial z} \text{ for } u \gg v. \tag{27}$$

It is interesting to note that the experimentally determined value of the dimensionless coefficient K in (27) agrees with the largely used drag coefficient C_d, generally accepted to lie in the range ~0.001–0.01 [*Parker et al.*, 1986; *Rowland*, 2007].

6. Analytic Solutions for PV

[37] From the definition of PV (19) and the physical and empirical assumptions made in section 5 (equations (25) and (27)), we can write the steady state *Ertel* [1942] PV theorem (20) for the approximate case $u \gg v$ as

$$\frac{d}{dt}\Pi_c = u\frac{\partial \Pi_c}{\partial x} = -2\frac{Ku}{\rho h}\left(\frac{\partial u}{\partial z}\frac{\partial c}{\partial y} + \zeta\frac{\partial c}{\partial z}\right), \tag{28}$$

which gives

$$\frac{\partial}{\partial x}\Pi_c = -2\frac{K}{h}\Pi_c. \tag{29}$$

Despite its simplicity, this new equation (29) provides insight into the along-stream evolution of PV. First, for inertia-dominated flow sensu *Wright* [1977], where frictional effects are small (i.e., deep outlet), it immediately results from equation (29) that the PV of the system is a conserved quantity. This is in agreement with the main feature of this kind of jet, that is the constant and low spreading angle [*Wright*, 1977]. This characteristic can be seen as the ability of the system to keep the pronounced Gaussian shape of the horizontal velocity profile, without "deforming" such a pattern (Figures 5, 6, 7, and 8; see below for more explanation).

[38] Moreover, *Rowland* [2007] and *Rowland et al.* [2009a], based on prior stability analysis of similar flows, argued that for systems that give rise to elongate channels, a decrease in flow thickness, which physically corresponds to an increase in internal friction of the flow, tends to damp the meandering of the flow and thus to decrease the lateral transport of sediment. This two-dimensional process may be encoded in the one-dimensional formulation (29).

[39] Following equation (23) and thus scaling the PV as

$$\Pi_c \approx 2\frac{\Delta U}{\Delta B}\frac{\Delta c}{\Delta h} \approx \frac{U}{B}\frac{C}{h}, \tag{30}$$

one can see that decreasing h must cause a decrease in vorticity due to the lateral shearing (i.e., $\zeta \approx \frac{U}{B}$) in order to conserve PV, which in turn would decrease sedimentation at the lateral margins of the jet and thus enhance deposition in front of the river mouth (Figure 7). This result highlights the connection between the vertical component of the jet vorticity ζ (referred to as "vorticity" hereafter) and the movement of sediments toward the margins, providing physical justification for the empirically determined relation between the lateral diffusivity coefficient and the flow depth, $k_y = 0.13hu^*$ [*Fischer*, 1973].

[40] In a more general situation, where bed friction has to be taken into account, equation (29) has the classical solution

$$\frac{d\Pi_c}{\Pi_c} = -2\frac{K}{h}dx \Rightarrow \Pi_c(x,y) = \Pi_c(x=0,y)\exp\left(-2\frac{K}{h}x\right), \tag{31}$$

where both K and h are reasonably considered as constants. From equation (31) one can note that Π_c is considerably reduced at $x = \frac{3h}{2K} \approx h10^3$ m, which confirms that for the study systems (Table 1) and for $K = C_d \sim 0.005$, the PV is not significantly damped along stream. Such a length scale relation may also give some insight about the ZOFE length scale, within which the vorticity of the system remains fairly constant, contributing sediment deposition along the margin of the jet while avoiding frontal bar formation.

[41] All this suggests that, in any case, PV is a rather conserved quantity as in many other oceanographic and meteorologic applications [*Gill*, 1982; *Pedlosky*, 1987]. We however remark that the stronger assumption $\nabla\Psi \approx 0$, related to the ability of the system to keep sediment in suspension, is principally responsible for such PV conservation. These results indicate that the fundamental parameter controlling the occurrence of elongate channels is the initial value of PV at the channel outlet. In synthesis, if a strong PV, and thus a strong vorticity, is recognized at the outlet, then the jet will tend to propagate without losing its PV. Such a jet will assume the behavior of a filament, characterized by a weak flattening and widening downstream due

to shearing and lateral mixing with ambient water at the jet margins. All this is consistent with available theoretical and field observations, and appears to explain key aspects of levee deposition [*Rowland*, 2007; *Rowland et al.*, 2009a].

7. Observed Jets and Filaments From Satellites

[42] In order to provide a validation for our PV hypothesis that the occurrence of elongate channels is related to jet/filament characteristics of the out flow, we analyze satellite images of several representative river jets. In physical oceanography, thermal and ocean-color satellite imagery has allowed considerable progress in the observation and modeling of transient jets, or cold filaments, observed off of coastal areas. Several theoretical analyses [*Send*, 1989; *Grimshaw and Yi*, 1990, 1991] suggest that dynamics of these filaments are related to the presence of PV fronts and their instabilities due to a topographic slope. *Holland* [1967] investigated high potential vorticity input into marine waters as generated by short-term wind bursts, which were funneled by the coastal orography into a restricted area of the sea surface near the coast. For such systems one has [*Holland*, 1967]

$$\frac{d\Pi_h}{dt} = -\frac{1}{\rho} curl\left(\frac{\bar{\tau}}{\rho h}\right), \tag{32}$$

where the arbitrary function for PV is $\lambda = h$. Equation (32), which looks rather similar to our formulation in equation (29), shows how the PV evolution (i.e., $\frac{d\Pi_h}{dt}$) is inversely proportional to h^2. Indeed, it has been observed that a funneled wind over the shallowest part of the shelf gives rise to the highest PV input into marine waters; such strong and localized PV inputs do not remain confined to the coastal zone, but are propagated offshore as filaments or jets [*Bignami et al.*, 2008].

[43] To investigate the dynamics described above, *Bignami et al.* [2008] examined NOAA Advanced Very High Resolution Radiometer (AVHRR) thermal satellite images of cold filaments in the Mediterranean Sea, which may be considered high PV structures. Figure 4 shows an example of a thermal satellite image (17 September 1998) of SE Sicily where a cold filament entering the Ionian Sea is easy to recognize. It is clear that this filament has only limited mixing with ambient water.

[44] Although occurring at a different scale, we recognize a similar pattern at the Southwest Pass of the Mississippi birdsfoot outlet (Figure 9). Sea surface temperature (SST) images have been collected for both Wax Lake and Mississippi birdsfoot Delta basins. We selected images of river plumes taken during high discharge events occurring simultaneously in both channels (Figures 9 and 10), where SST may be used as a flow tracer. From this analysis it is clear that the two channels have very different flow patterns (Figure 9). Outflow from Southwest Pass clearly shows properties of a high-PV system, in which limited mixing allows the river outflow to penetrate deeply into the basin as a coherent jet. Wax Lake, on the other hand, shows no filament pattern (Figure 9). In this case the riverine water tends to remain confined to the coastal area, a feature that may suggest low PV at the outlet.

[45] A similar pattern can be recognized in the horizontal distribution of suspended sediment at the two study outlets. *Myint and Walker* [2002] quantified near-surface suspended sediment concentrations using data acquired by the NOAA/AVHRR and the Orbview-2 Sea-viewing Wide Field-of-view Sensor (SeaWiFS) ocean color sensor, coupled with field measurements. A similar approach, involving also theoretical solutions for a 2-D turbulent jet, was given in *Peckham* [2008]. Results from the *Myint and Walker* [2002] model (Figure 11) clearly show that the filament behavior of the Southwest Pass observed from SST images is also recognizable in the suspended sediment distribution. It appears that a high-PV system may transport sediment offshore with little deposition in front of the river, and thus is not likely to give rise to bifurcating channels. Large values for lateral sediment diffusivity associated with high-PV systems (as outlined above) may favor rapid levee deposition and the growth of elongate channels.

[46] In order to explain the counterintuitive fact that a high-PV jet can maintain its Gaussian shape without much spreading/mixing, we need to consider that a highly stratified jet (in terms of suspended sediment concentration) with a pronounced Gaussian horizontal velocity profile (i.e., a high-PV system) will not lose sediment, and thus momentum, at its centerline if $u^* \gg u_c^*$ (Figure 7). Although there are eddies being shed off the jet that construct the levees, within a certain distance from the outlet the Gaussian shape of the jet is not diffused since the centerline velocity is not decreasing rapidly, in particular if $\frac{d\Pi_c}{dt} = 0$. With this pattern, the lateral gradient of suspended sediment concentration is still high and looks like that of the horizontal velocity. This feature is experimentally observed in the proximal portion of the jet (Figure 6) as reported by *Rowland* [2007] and *Rowland et al.* [2010]. Somehow, all this reveals that the system can spread water and sediment toward the lateral boundaries without spreading PV, as confirmed by theoretical works of *Haynes and McIntyre* [1987] and *Marshall et al.* [2001]. This hydrodynamic "self-propagation" occurs in filament-like jets until the friction totally "erases" the PV of the system, at a distance that is likely related to the ZOFE.

8. Bulk Vorticity and PV for Natural and Experimental Systems

[47] Our analysis suggests that bifurcating channels, such as Wax Lake and the numerical simulations of *Edmonds and Slingerland* [2007], should have relatively low PV. The more elongate channels of the Mississippi birdsfoot, and in particular Southwest Pass, should have higher values for PV. Tie channels are the most elongate channels known (Figure 3), and we hypothesized earlier that they are end-members of the birdsfoot morphology; these systems, and the experimental jets designed by Rowland [*Rowland*, 2007; *Rowland et al.*, 2009a, 2010] to simulate them, are expected to have the highest PV values. Here we present a first analysis on scaling of PV (Π_c) across this range of channel morphologies.

[48] We used equation (30) in order to scale the PV and to provide bulk values for Π_c and ζ, scaled as $\Pi_c = \frac{U}{B}\frac{C}{h}$ and $\zeta = \frac{U}{B}$, respectively, at the channel outlet for all examples considered in this work. Different values for U, B, C and h related to numerical and experimental runs were taken

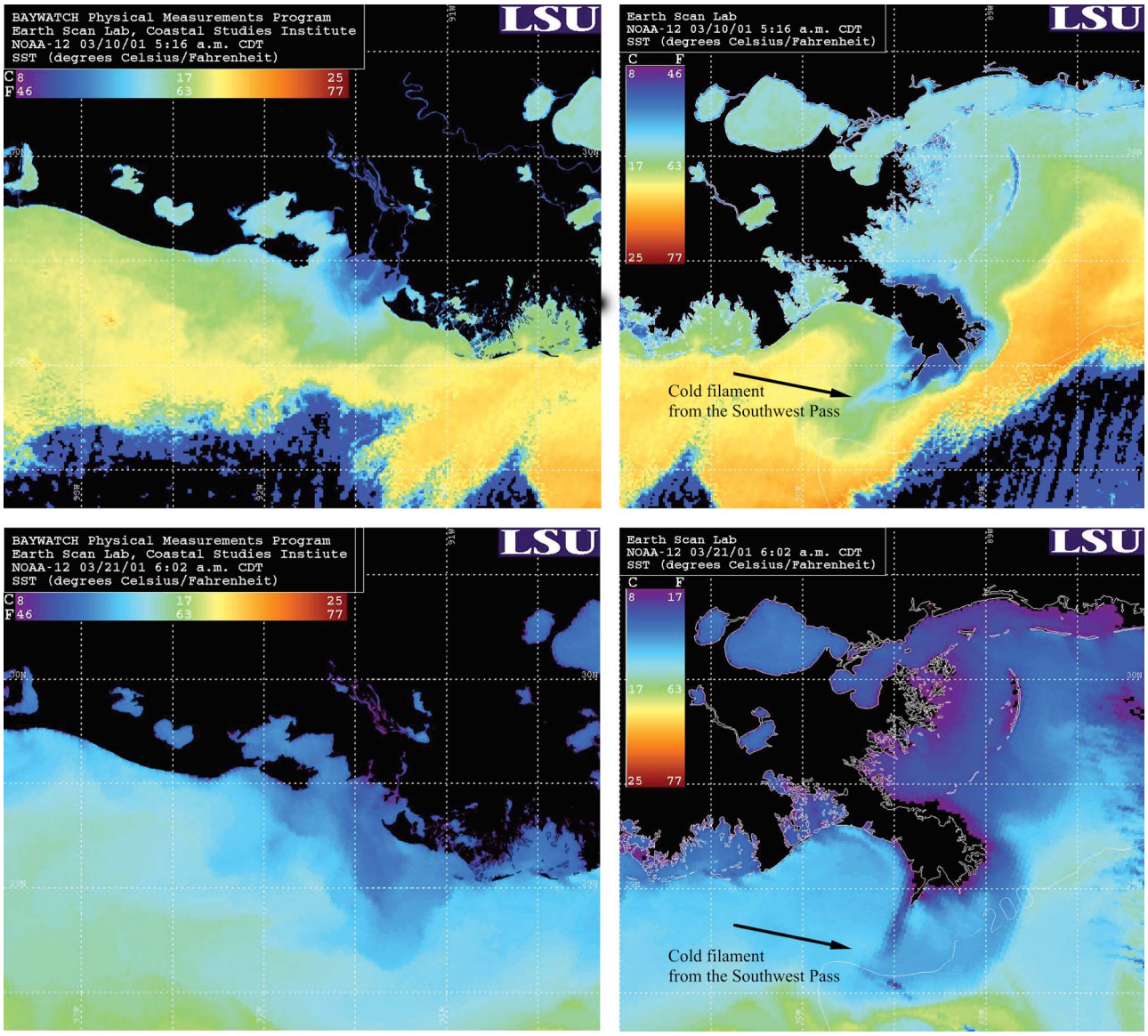

Figure 9. NOAA/AVHRR images of sea surface temperature from the two high-discharge events recognized on 10 and 21 March 2001, for the (left) Atchafalaya bay and (right) the Mississippi birdsfoot. Data were processed by the Earth Scan Lab (Coastal Studies Institute, Louisiana State University). Arrows indicate the cold filaments outflowing from the Southwest Pass of the Mississippi birdsfoot outlet.

from *Edmonds and Slingerland* [2007] and *Rowland et al.* [2009a], respectively (Table 1). *Rowland* [2007] also provided hydrologic and sedimentologic data for all analyzed tie channels (Table 1). This allowed us to give a more accurate estimate of Π_c and ζ, as shown in Table 2. Reported values of morphologic parameters for the Wax Lake and Southwest Pass channels are highly variable in the literature; we refer to those reported by *Buttles et al.* [2007] and the U. S. Army Corps of Engineers (http://www.mvn.usace.army.mil), respectively. Values for bulk jet velocity and suspended sediment concentration of these two channels must correspond to simultaneous high-discharge events, in order to directly compare formative hydrodynamic conditions between these systems. *Myint and Walker* [2002] obtained water samples on 21 March 2001 in the Atchafalaya Bay region and in the Mississippi River plume, coincident with a clear-sky NOAA AVHRR image and high discharge for both rivers (Figures 9 and 11). These observations provide bulk velocity and suspended sediment concentration (Table 1).

[49] We chose the Mississippi Delta as our natural example because of the remarkable difference in channel patterns between western (e.g., Wax Lake) and eastern (birdsfoot) branches of the same system, and the interest in using Wax Lake growth as a model for birdsfoot restoration [*Kim et al.*, 2009a]. Our interpretation of the relation between hydrodynamics and channel growth patterns is of course complicated, however, by the strong human influence on both channels, and therefore some justification of our analysis is warranted. For the Wax Lake Delta, we are interested in the initial channel mouth conditions that first led to branching, consistent with our hypothesis that initial

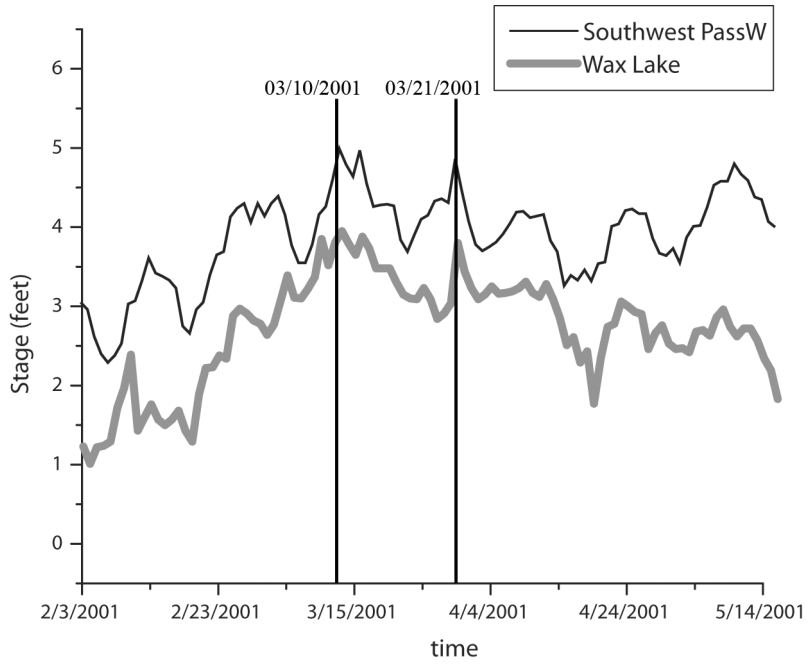

Figure 10. Time series of hydrologic stage data (Gauge Zero not provided) for the Southwest Pass of the Mississippi birdsfoot outlet and the Wax Lake. Data from U.S. Army Corps of Engineers, http://www.mvn.usace.army.mil/.

PV conditions at a river mouth determine whether future growth will be elongate of bifurcate. The dredging of Wax Lake and subsequent capture of Atchafalaya water and sediment initiated growth of the branching delta several decades ago [*Parker and Sequeiros*, 2006; *Kim et al.*, 2009a]. Therefore, PV was estimated using modern values for the feeder channel under the reasonable assumption that these conditions are similar to those at initiation. We do not

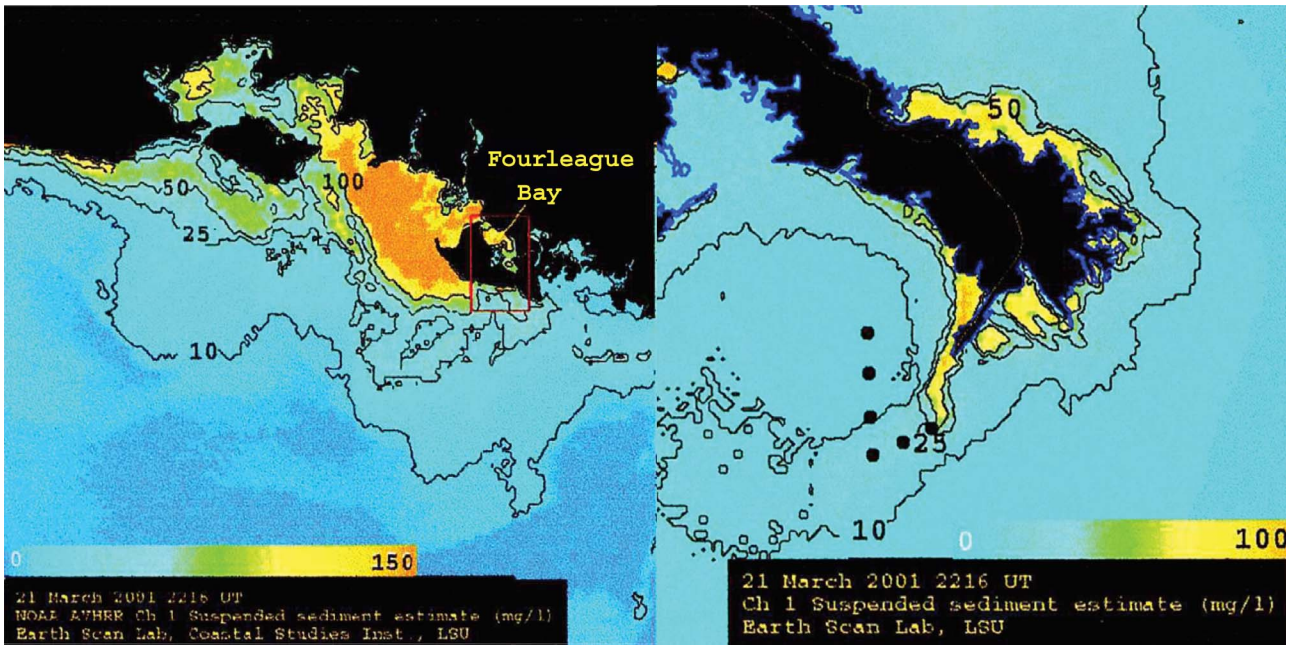

Figure 11. Model-estimated regional suspended sediment concentrations (mg/l) for the (right) Southwest Pass of the Mississippi birdsfoot and (left) the Wax Lake on 21 March 2001 [from *Myint and Walker*, 2002]. Contour lines are shown for 10, 25, 50, and 100 mg/l. The red box indicates the region in which "ground truth" data were obtained for calibration. The similarity between the suspended sediment patterns SST pattern (and thus the flow pattern) can be seen from the comparison with Figure 9.

estimate here the PV of the smaller branches; because channel geometry, fluid velocity and sediment concentration can change downstream, however, a branching delta likely exhibits spatial variations in PV. This introduces the interesting possibility that a delta may undergo transitions from elongate to bifurcating flow conditions, but this topic is beyond the scope of the current paper.

[50] For the birdsfoot, we chose Southwest Pass because it is the largest distributary and also exhibits the strongest and most coherent plume seen in satellite imagery. As discussed, the general elongate morphology of the birdsfoot existed before human intervention [*Fisk et al.*, 1954; *Kim et al.*, 2009a]. Surveys show that Southwest Pass in particular was also elongate even before constriction by levees and jetties, and may have been growing as a single elongating channel for the last 500 years [*Fisk et al.*, 1954]. However, the current channel is constricted by artificial levees and is also dredged for shipping, such that a direct link between formative flow conditions and channel morphology cannot be made. Nevertheless, we are able to make direct comparisons between the modern (engineered) Southwest Pass outflow conditions and the patterns of flow and suspended sediment of its plume. This comparison helps to confirm that a high-PV channel outlet generates a focused jet, regardless of how that channel outlet was constructed. Extrapolating Southwest Pass results to the entire birdsfoot cannot be quantitatively justified. It is not unreasonable however, based on available data, to assume that flow and channel geometry of the modern Southwest Pass are of the same order of magnitude as the (unknown) formative conditions for that channel [*Fisk et al.*, 1954], while its modern PV value might provide a minimum constraint for PV associated with formative conditions of the original birdsfoot feeder channel. Comparison of numerical values for PV (Tables 1 and 2) should be treated with appropriate caution.

[51] Results show that Wax Lake Delta has the lowest value for PV of all systems considered, and that PV for simulations of *Edmonds and Slingerland* [2007] is comparable (Table 2). The correspondence of low PV and a bifurcating morphology, and the good agreement for PV values between nature and simulations, indicates that bifurcating channel systems indeed form under conditions of low initial PV. From a rough estimation of $\zeta = \frac{U}{B}$ at the outlet, one can argue that jet spreading for these system generally shows a fairly low vorticity (Table 2), i.e., a flat horizontal velocity profile, which we hypothesize allows for the formation of a frontal bar in proximity of the river mouth. Estimated PV for Southwest Pass is one order of magnitude larger than that of Wax Lake (Table 2), indicating that bifurcation should be suppressed while levee deposition should be amplified. Indeed, the channel is likely artificially maintained in order to enhance the suppression of mouth bar deposition. As discussed, Southwest Pass displays a rather elongate morphology and has jet properties consistent with this interpretation (Figures 1, 2, and 9). A representative PV value for natural tie channels is one order of magnitude larger than Southwest Pass, consistent with a strongly focused jet and our interpretation that this morphology is an end-member for elongate channel systems (Table 2). Finally, *Rowland et al.* [2009a] experiments have PV values that are two orders of magnitude larger than natural tie channels. Such high PV, given by a high vorticity of this experimental run, acts to maximize delivery of sediment to the margins of the jet, where values for shear velocity are lower (Figure 7). We remark that this can be explained by considering that high vorticity systems show a very pronounced Gaussian horizontal velocity profile. This shape, which is reflected in the shear velocity profile (Figure 7), clearly damps frontal bar aggradation while promoting strong sedimentation at the lateral boundaries.

[52] We can explain the ability of a high-PV system to favor deposition at jet margins in a more analytical way, by considering the relation between lateral shear stress and lateral momentum diffusivity that was pointed out by *Rowland et al.* [2009a]. They estimated the momentum diffusivity k^y by means of the $-\overline{u}'v'$ component of the Reynolds stress and determined experimentally a dependence between the lateral shear stress and momentum diffusivity:

$$\tau_{uv} = \rho k^y \frac{\partial u}{\partial y} \approx \rho k^y \zeta. \tag{33}$$

[53] Equation (33) clearly shows how the vorticity of the system is involved in the transfer of momentum across the jet. Experiments also showed that both the lateral diffusivity (33) [*Rowland et al.*, 2009a] and the lateral transfer of sediment [*Rowland*, 2007] are connected with the meandering features of jets; jet meanders are observed both in natural tie channels and in experiments (Figure 1). Although consideration of these transient flow features is beyond the scope of the analytical approach presented here, our steady state solution and equation (33) predict a time-averaged relation between vorticity and levee growth that supports these experimental observations.

9. Discussion and Conclusions

[54] *Kim et al.* [2009b] constructed a model for river delta growth resulting from a sediment source that progrades at a constant velocity into a quiescent basin. Their results showed how the degree of channel elongation is controlled by the river mouth progradation rate, which must be related somehow to the process of levee building. *Kim et al.* [2009b] did not model this process, however they offered suggestions for the requisite conditions of elongate channels that are relevant here: (1) localized deposition of levees at the river mouth and (2) the presence of mud/cohesive sediment to preserve an elongate form. The numerical study by *Edmonds and Slingerland* [2010] explicitly examined the control of sediment cohesion (i.e., mud) on channel morphology.

[55] Experiments with noncohesive sediment demonstrate that subaqueous levee deposition does not require cohesion [*Rowland*, 2007], however it may affect channel development as proposed by *Kim et al.* [2009b] and *Edmonds and Slingerland* [2010]. Clearly cohesion is not explicitly considered in our model, however the PV formulation allows us to explore potential effects cohesion may have on channel growth. One important effect of cohesion on sediment is that the critical stress for entrainment is significantly larger than that of deposition. In addition, it is well known that channels in cohesive sedimentary environments are narrower and deeper than channels cut into noncohesive sediments [*Rowland et al.*, 2009b], because coarse-grained bed load

has a lower critical entrainment stress than cohesive sediment banks [*Parker*, 1978]. Cohesion may therefore enhance elongation by two processes that have not been considered in previous models: (1) lack of reentrainment of deposited grains enhances potential vorticity by equation (20) and thus promotes filament jet behavior, and (2) cohesion leads to the formation of relatively narrow and deep channels, creating initial conditions of high vorticity at the river mouth. Confirmation of these ideas requires further field work and numerical modeling.

[56] We now consider our results in light of recent proposals to construct land via artificial diversions on the Balize lobe of the Mississippi River Delta downstream of New Orleans [*Parker and Sequeiros*, 2006; *Kim et al.*, 2009a], which aim to reverse coastal erosion and wetland loss in the vicinity [*Blum and Roberts*, 2009; *Kim et al.*, 2009a]. A plan to divert Mississippi River water and sediment through levee breaches 150 km downstream of New Orleans is gaining traction [*Kim et al.*, 2009a]. The proposed diversions would promote sediment deposition at the margins of the channel, resulting in the growth of deltaic lobes into surrounding bays. The current model uses Wax Lake as the ideal morphology and the prototype for how an artificial delta will grow [*Kim et al.*, 2009b], however current flow and sediment conditions on the Balize lobe favor elongate channel formation (Figures 1 and 2). Because the initial hydrodynamics of a river mouth appear to determine the eventual shape of a channel, however, it seems reasonable that levee cuts may be designed to select a preferred growth pattern. We propose that potential vorticity may be a useful scale parameter in the design of artificial land growth. If bifurcating, radial delta growth is the desired outcome, then initial channel geometry, flow velocity and sediment concentration may be chosen such that potential vorticity matches that observed for branching channel systems such as Wax Lake. At the very least, this idea may be tested through detailed numerical simulations such as Delft3D, in which a suite of numerical experiments may be performed having a range of potential vorticity values. We finally remark that the proposed scaling for potential vorticity in equation (30) appears to be a ratio of sediment discharge and cross-sectional area of the channel outlet, emphasizing how upstream channel geometry controls potential vorticity conditions at the outlet.

[57] In conclusion, we have derived a hydrodynamic theory that describes flow and sediment concentration patterns for a turbulent river jet entering quiescent water. By choosing sediment concentration as a nonconserved scalar property of the flow, we derived a new potential vorticity using the *Ertel* [1942] theorem that predicts sedimentation downstream of a river mouth as a result of initial conditions at the mouth. As known from physical oceanography, high-PV jets preserve their filament shape because of minimal mixing with ambient water at jet margins [*Holland*, 1967; *Haynes and McIntyre*, 1990; *Bignami et al.*, 2008]. For high-PV sediment-laden riverine jets this feature can be seen as the ability of the system to maintain a well pronounced Gaussian horizontal velocity profile (and the related horizontal shear stress), which limits sediment deposition along the jet centerline as confirmed in recent experimental works. The result is that systems with high PV have rapid levee deposition relative to frontal mouth bar growth, producing elongate channels. In such a condition the mouth bar would prograde downstream since the high shear stress at the jet centerline damps any vertical aggradation. This is reflected in the vorticity of the system that was found to be related to the horizontal distribution of the boundary shear stress and to the momentum diffusivity. Comparison with the limited field, laboratory and numerical data that are available supports the suggestion that potential vorticity is a primary control on channel pattern. Sediment cohesion has an additional, relatively unexplored effect that we were unable to incorporate here. It seems possible that cohesion actually enhances elongation through maintaining potential vorticity.

[58] Potential vorticity alone cannot describe all of the relevant dynamics of jet sedimentation. In particular, a crucial second component is the magnitude of shear stresses in the jet compared to the critical stress for sediment entrainment (Figure 7). Suspended sediment from the jet will deposit only where stresses are lower than the critical value [*Rowland et al.*, 2010]. It is possible in theory that a jet could have high PV, but not create focused levee deposition simply because shear stress everywhere in the jet is lower than the critical value. For natural systems, however, it appears that high-PV systems are also systems of (relatively) large shear stress in the jet centerline, such that the joint conditions of high PV and above-threshold shear stress are met simultaneously and lead to elongate channel growth. This is not necessarily the case in laboratory experiments, where PV and critical stress may be independently varied. Future exploration of the joint controls of PV and critical shear stress on jet sedimentation therefore seem particular well suited to an experimental approach. The PV formulation helps to describe the spatial structure of bed shear stresses for a sediment-laden jet; further theoretical and experimental work that solidifies this linkage would be most useful.

[59] The current model represents a theoretical framework, but it is not complete. Empirical closures for sediment concentration distribution, external forces such as bed friction and lateral entrainment, and lateral momentum diffusivity were needed, but it is not known how generally applicable experimentally derived values are. Our conclusions thus remain primarily qualitative at present. Nevertheless, the potential vorticity model serves to collect the relevant processes that govern river mouth deposition into a compact framework, which may serve as a point of departure for future theoretical, numerical and empirical studies; it may also be a starting point for designing diversion structures associated with delta land-building schemes.

Notation

L	bulk channel length (m).
B	bulk channel width (m).
h	channel (flow) depth (m).
$\vec{u} = (u, v, w)$	flow velocity (m/s).
$\vec{\Omega}$	Earth's angular velocity (s^{-1}).
ρ	flow density (kg/m^3).
p	fluid pressure (N/m^2).
φ	potential of the gravity force (m^2/s^2).
$\vec{F}$	external forces per unit volume (N/m^3).
f	coriolis parameter (s^{-1}).

τ_{xij}	fluid shear stresses (N/m^2).
c	mass suspended sediment concentration (kg/m^3).
$\vec{k}_s = (k^x_{sed}, k^y_{sed}, k^z_{sed})$	sediment eddy diffusivity coefficient (m^2/s).
$\vec{k} = (k^x, k^y, k^z)$	momentum diffusivity coefficient (m^2/s).
u_c	jet centerline velocity (m/s).
w_s	hindered sediment settling velocity (m/s).
$G(y)$	Gaussian similarity function.
E_w	entrainment coefficient.
U	along-stream depth-averaged velocity (m/s).
V	cross-stream depth-averaged velocity (m/s).
γ	streamwise velocity decay rate constant.
q	lateral spreading coefficient.
$u*$	shear velocity (m/s).
C_d, K	mean coefficient of friction.
$\vec{\omega} \approx (0, \psi, \zeta)$	flow vorticity (s^{-1}).
Π_c	potential vorticity (s^{-1}/m).

[60] **Acknowledgments.** We thank J. Rowland, D. Edmonds, and E. Salusti for sharing their insights and data. We gratefully acknowledge support by the National Science Foundation through contract EAR-0746138 to D.J.J. This work was inspired by discussions at the Doolin "deltas workshop" with A. Fowler, C. Stark, J. Swenson, and V. Voller, sponsored by the National Center for Earth-Surface Dynamics. The authors also thank C. Paola for providing further insights about the physical interpretation of our work.

References

Abramovich, G. N. (1963), *Theory of Turbulent Jets*, 684 pp., MIT Press, Cambridge, MA.

Albertson, M. L., Y. B. Dai, R. A. Jensen, and H. Rouse (1950), Diffusion of submerged jets, *Trans. Am. Soc. Civ. Eng.*, *115*, 639–664.

Bates, C. C. (1953), Rational theory of delta formation, *AAPG Bull.*, *37*(9), 2119–2162.

Bignami, F., E. Böhm, E. D'Acunzo, R. D'Archino, and E. Salusti (2008), On the dynamics of surface cold filaments in the Mediterranean Sea, *J. Mar. Res.*, *74*, 429–442.

Blum, M. D., and H. H. Roberts (2009), Drowning of the Mississippi Delta due to insufficient sediment supply and global sea-level rise, *Nat. Geosci.*, *2*, 488–491, doi:10.1038/ngeo553.

Buttles, J., D. Mohrig, J. Nittrouer, B. McElroy, E. Baitis, M. Allison, C. Paola, G. Parker, and W. Kim (2007), Partitioning of Water Discharge by Distributary Channels in the Prograding, Wax Lake Delta, Coastal Louisiana, *USA. Eos Trans. AGU*, *88*(52), Fall Meet. Suppl., Abstract H54A–02.

Dracos, T., M. Giger, and G. H. Jirka (1992), Plane turbulent jets in a bounded fluid layer, *J. Fluid Mech.*, *241*, 587–614, doi:10.1017/S0022112092002167.

Edmonds, D. A., and R. L. Slingerland (2007), Mechanics of middle-ground bar formation: Implications for the morphodynamics of delta distributary networks. *J. Geophys. Res.*, *112*, F02034, doi:10.1029/2006JF000574.

Edmonds, D. A., and R. L. Slingerland (2010), Significant effect of sediment cohesion on delta morphology, *Nat. Geosci.*, *3*, 105–109, doi:10.1038/ngeo730.

Ellison, T., and J. Turner (1959), Turbulent entrainment in stratified flows, *J. Fluid Mech.*, *6*, 423–448, doi:10.1017/S0022112059000738.

Ertel, H. (1942), Ein neuer hydrodynamischer Wirbelsatz, *Meteorol. Z.*, *59* (2), 277–281.

Fischer, H. B. (1973), Longitudinal dispersion and turbulent mixing in open-channel flow, *Annu. Rev. Fluid Mech.*, *5*, 59–78, doi:10.1146/annurev.fl.05.010173.000423.

Fisk, H. N., C. R. Kolb, E. McFarlan, and L. J. Wilbert (1954), Sedimentary framework of the modern Mississippi delta, [Louisiana], *J. Sediment. Res.*, *24*(2), 76–99.

Giger, M., T. Dracos, and G. H. Jirka (1991), Entrainment and mixing in plane turbulent jets in shallow-water, *J. Hydraul. Res.*, *29*(5), 615–642, doi:10.1080/00221689109498980.

Gill, A. E. (1982), *Atmosphere-Ocean Dynamics*, *Int. Geophys. Ser.*, vol. 30, Academic, San Diego, Calif.

Grimshaw, R., and Z. Yi (1990), Finite amplitude long-waves on coastal currents, *J. Phys. Oceanogr.*, *20*, 3–18, doi:10.1175/1520-0485(1990)020<0003:FALWOC>2.0.CO;2.

Grimshaw, R., and Z. Yi (1991), Evolution of a potential vorticity front over a topographic slope, *J. Phys. Oceanogr.*, *21*, 1240–1255, doi:10.1175/1520-0485(1991)021<1240:EOAPVF>2.0.CO;2.

Haynes, P. H., and M. E. McIntyre (1987), On the evolution of vorticity and potential vorticity in the presence of diabatic heating and frictional or other forces, *J. Atmos. Sci.*, *44*, 828–841, doi:10.1175/1520-0469(1987)044<0828:OTEOVA>2.0.CO;2.

Haynes, P. H., and M. E. McIntyre (1990), On the conservation and the impermeability Theorems for Potential Vorticitiy, *J. Atmos. Sci.*, *47*, 2021–2031, doi:10.1175/1520-0469(1990)047<2021:OTCAIT>2.0.CO;2.

Holland, W. R. (1967), On the wind-driven circulation in an ocean with bottom topography, *Tellus*, *19*, 582–600, doi:10.1111/j.2153-3490.1967.tb01510.x.

Holton, J. R. (1992), *An Introduction to Dynamic Meteorology*, *Int. Geophys. Ser.*, vol. 48, Academic, San Diego, Calif.

Jerolmack, D. J., and J. B. Swenson (2007), Scaling relationships and evolution of distributary networks on wave-influenced deltas, *Geophys. Res. Lett.*, *34*(23), L23402, doi:10.1029/2007GL031823.

Kim, W., D. Mohrig, R. Twilley, C. Paola, and G. Parker (2009a), Is it feasible to build new land in the Mississippi River delta?, *Eos Trans. AGU*, *90*(42), 373–374, doi:10.1029/2009EO420001.

Kim, W., A. Dai, T. Muto, and G. Parker (2009b), Delta progradation driven by an advancing sediment source: Coupled theory and experiment describing the evolution of elongated deltas, *Water Resour. Res.*, *45*, W06428, doi:10.1029/2008WR007382.

Marshall, J., D. Damous, and J. Nilsson (2001), Entry, flux, and exit of potential vorticity in ocean circulation, *J. Phys. Oceanogr.*, *31*, 777–789, doi:10.1175/1520-0485(2001)031<0777:EFAEOP>2.0.CO;2.

Muller, P. (1995), Ertel's potential vorticity theorem in physical oceanography, *Rev. Geophys.*, *33*(1), 67–97, doi:10.1029/94RG03215.

Myint, S. W., and N. D. Walker (2002), Quantification of surface suspended sediments along a river dominated coast with NOAA AVHRR and SeaWiFS measurements: Louisiana, USA, *Int. J. Remote Sens.*, *23*, 3229–3249, doi:10.1080/01431160110104700.

Necker, F., C. Härtel, L. Kleiser, and E. Meiburg (2002), High-resolution simulations of particledriven gravity currents, *Int. J. Multiphase Flow*, *28*, 279–300, doi:10.1016/S0301-9322(01)00065-9.

Parker, G. (1978), Self-formed straight rivers with equilibrium banks and mobile bed. Part 1. The sand-silt river, *J. Fluid Mech.*, *89*, 109–125, doi:10.1017/S0022112078002499.

Parker, G., and O. Sequeiros (2006), Large scale river morphodynamics: Application to the Mississippi Delta, paper presented at River Flow 2006: International Conference on Fluvial Hydraulics, Inst. Super. Tec., Lisbon.

Parker, G., Y. Fukushima, and H. M. Pantin (1986), Self-accelerating turbidity currents, *J. Fluid Mech.*, *171*, 145–181, doi:10.1017/S0022112086001404.

Peckham, S. D. (2008), A new method for estimating suspended sediment concentrations and deposition rates from satellite imagery based on the physics of plumes, *Comput. Geosci.*, *34*(10), 1198–1222, doi:10.1016/j.cageo.2008.02.009.

Pedlosky, J. (1987), *Geophysical Fluid Dynamics*, Springer, New York.

Rajaratnam, N. (1976), *Turbulent Jets. Developments in Water Science*, Elsevier, Amsterdam.

Rowland, J. C. (2007), Tie channels, Ph.D. thesis, Univ. of Calif., Berkeley.

Rowland, J. C., M. T. Stacey, and W. E. Dietrich (2009a), Turbulent characteristics of a shallow wall-bounded plane jet: Experimental implications for river mouth hydrodynamics, *J. Fluid Mech.*, *627*, 423–449, doi:10.1017/S0022112009006107.

Rowland, J. C., W. E. Dietrich, G. Day, and G. Parker (2009b), Formation and maintenance of single-thread tie channels entering floodplain lakes: Observations from three diverse river systems, *J. Geophys. Res.*, *114*, F02013, doi:10.1029/2008JF001073.

Rowland, J. C., W. E. Dietrich, and M. T. Stacey (2010), Morphodynamics of subaqueous levee formation: Insights into river mouth morphologies arising from experiments, *J. Geophys. Res.*, *115*, F04007, doi:10.1029/2010JF001684.

Schlichting, H. (1968), *Boundary-Layer Theory*, McGraw-Hill, New York.

Send, U. (1989), Vorticity and instabilities during flow reversal on the continental shelf, *J. Phys. Oceanogr.*, *19*, 1620–1633, doi:10.1175/1520-0485(1989)019<1620:VAIDFR>2.0.CO;2.

Syvitski, J., K. Skene, M. Nicholson, and M. Morehead (1998), Plume 1.1: Deposition of sediment from a fluvial plume, *Comput. Geosci.*, *24*(2), 159–171, doi:10.1016/S0098-3004(97)00084-8.

Tennekes, H., and J. L. Lumley (1972), *A First Course in Turbulence*, MIT Press, Cambridge, Mass.

Turner, J. S. (1986), Turbulent entrainment: The development of the entrainment assumption, and its application to geophysical flows, *J. Fluid Mech.*, *173*, 431–471, doi:10.1017/S0022112086001222.

Wang, F. C. (1984), The dynamics of a river-bay-delta system, *J. Geophys. Res.*, *89*, 8054–8060, doi:10.1029/JC089iC05p08054.

Wright, L. D. (1977), Sediment transport and deposition at river mouths: A synthesis, *Geol. Soc. Am. Bull.*, *88*, 857–868, doi:10.1130/0016-7606(1977)88<857:STADAR>2.0.CO;2.

F. Falcini and D. J. Jerolmack, Department of Earth and Environmental Science, University of Pennsylvania, 240 S. 33rd St., Philadelphia, PA 19104-6316, USA.